

Matrix-Isolation FT-IR Studies and *ab Initio* Calculations of Hydrogen-Bonded Complexes of Molecules Modeling Cytosine or Isocytosine Tautomers. 4. H-Bonded Complexes of 1-Methyl-2-pyrimidone and *N,N*-1-Trimethylcytosine with Water

Johan Smets,[†] Alain Destexhe,[†] Ludwik Adamowicz,^{*,‡,§} and Guido Maes^{*,†}

Department of Chemistry, University of Leuven, Celestijnenlaan 200F, B-3001 Heverlee, Belgium, and
Department of Theoretical Chemistry, University of Lund, Lund S-22100, Sweden

Received: December 11, 1996; In Final Form: April 3, 1997[®]

We continue our combined experimental and theoretical *ab initio* studies of hydrogen-bonded complexes involving molecules modeling cytosines by investigating the H-bond interaction of 1-methyl-2-pyrimidone and *N,N*-1-trimethylcytosine with water. The objective of the present work is theoretical and spectral characterization of the base–water complexes in the argon matrix, where the water molecule can become hydrogen bonded to the base through two H bonds with hydrogens of both bonds coming from the water molecule. For the 1-methyl-2-pyrimidone base, the *ab initio* calculations predict the H-bonded complex at the N₃ site to be slightly more stable than the alternative complex at the C₂=O site. Both H-bonded complexes have a second, weaker H bond between the other water OH group and the C₂=O or N₃ base site. The predicted vibrational spectra of the two complexes do not match well with the observed experimental FT-IR spectrum. Possible reasons for the discrepancies between the experiment and the theory attributed to the presence of argon are discussed. While the theory predicts two closed complexes, each containing a double hydrogen bond, from the experimental spectrum, two open complexes at the C₂=O and N₃ interaction sites are identified. H-bonding of water with *N,N*-1-trimethylcytosine can occur at either the N₃, C₂=O, or (CH₃)₂N site. The stability difference between the first two complexes is relatively small, and the second H bond in both complexes is considerably weaker than in the pyrimidone complexes. As results from the calculations, the H-bond interaction at the methylated amino group is much weaker than the H bonds formed with N₃ and C₂=O, and this finds conformation in the experimental matrix spectra, where the spectral signature of this complex is absent. The relative frequency shifts and the ratios between the calculated and measured frequency values for the stretching mode of the bonded water for all the complexes of both basis are discussed in relation to the earlier established correlations for similar H-bonded complexes. Water-rich matrices contain also 1:2 complexes B···HO(H)···HOH. It is found that the central H bond in these linear structures is characterized by the cooperativity factor of 1.3–1.4.

Introduction

Biological reactions occur in environments which can have a profound influence on the progress and the outcome of the reactions. A network of weak interactions extends from the surrounding molecules toward the reactants forming conditions which are significantly different from the gas-phase environment. Particularly, hydrogen bonds are among those interactions which strongly connect oxygen- and nitrogen-rich biomolecules to the environment. Interaction with water plays a particularly important role in this phenomenon.

Hydrogen bondings involving a water molecule can be supported either by the water hydrogens or by the lone electron pairs of oxygen. There is a possibility that a single water molecule is engaged in a double hydrogen bond with a biomolecule where either both water hydrogens or one hydrogen and one electron pair participate in the interaction. In the present study, we investigate the former situation at the molecular level with the use of IR spectral and theoretical methods. This approach provides a unique insight into the structure and energetics of the double hydrogen bond formation, which is not

available in other experimental techniques. In particular, we investigate the question of hydrogen-bond cooperativity and anticooperativity which is essential in understanding the biological functioning of the hydrogen-bond network.

This paper is a part of the series of reports presenting experimental matrix-isolation FT-IR study combined with theoretical *ab initio* calculations aimed to interpret the vibrational spectra of water-complexed cytosines and isocytosine.^{1–4} In this report we describe the 1:1 H-bonding interaction of water with 1-methyl-2-pyrimidone (MOP) and *N,N*-1-trimethylcytosine (TMC) in the inert low-temperature Ar matrix environment. TMC (Scheme 2) is one of the simplest cytosine derivatives suitable for investigating H-bond characteristics of cytosines, since the number of possible H-bonded complexes is strongly reduced in comparison with cytosine. While the latter compound occurs as a mixture of three tautomers in Ar,^{5–6} the hydroxy–oxo and amino–imino prototropies are blocked in TMC by substitution of all the protomeric hydrogen atoms at N₁ and at the amino N atom by methyl groups. As a consequence, water can only act as a proton donor toward this base and form either C₂=O···HO–H or N_i···HO–H (*i* = 3, 14) complexes. Formation of H-bonded complexes at C₂=O or N₃ is also possible in the case of MOP (Scheme 1) which differs from TMC by the absence of the dimethylamino group. Furthermore, the influence of the amino group on the basicity of the N₃ and C₂=O sites in cytosines can be evaluated by a comparison of the H-bond characteristics of the two compounds

* Corresponding author. Senior Research Associate of the Belgian National Fund for Scientific Research.

[†] University of Leuven.

[‡] University of Lund.

[§] Permanent address: Department of Chemistry, University of Arizona, Tucson, AZ 85721.

[®] Abstract published in *Advance ACS Abstracts*, July 15, 1997.

investigated here. We should note that the model molecules presented in this work differ from those described earlier. In MOP and TMC the N_3 and $C_2=O$ interaction centers are situated very close to each other and will compete as proton acceptors toward the water molecule. It is possible that in complexes with these compounds, water can be a double proton donor and form a complex with two H bonds at the two proton-accepting interaction centers. In the model molecules described in the former parts of this series, the H-bond interaction centers were more separated and/or acted in opposite ways toward the water molecule, *i.e.*, one as a proton acceptor and the other one as a proton donor.

The present results will be used in the future interpretation of the FT-IR spectra of complexes between water and the oxo tautomers of 1-methylcytosine⁷ and cytosine/isocytosine.⁸ In particular, the vibrational characteristics of the H-bonded complexes of the presently studied methylated compounds will allow us to distinguish between open and the closed complex structures, the latter being preferably formed by non-methylated derivatives with vicinal H-bonding interaction sites of opposite nature, *e.g.*, 2-hydroxypyridine, 2- and 4-hydroxypyrimidine, or cytosines/isocytosine. Using rotationally resolved electronic spectroscopy, Held and Pratt observed closed 1:1 and 1:2 complexes of 2-hydroxypyridine and water in the gas phase,⁹ while Del Bene has reported *ab initio* MP2/cc-pVTZ+//MP2/6-31+G** results for the 1:1 complex.¹⁰ *Ab initio* calculations of the proton-transfer barrier in the free and H-bonded 2-hydroxypyridines indicated a noticeable decrease of the barrier in the H-bonded form of the base in comparison with the free form,¹¹ which suggests a "H-bond assisted" mechanism for prototropy in this kind of tautomeric system. As a matter of fact, we will demonstrate in subsequent reports that doping Ar matrices with water induces a shift of the position of the hydroxy \rightarrow oxo tautomeric equilibrium in isolated 2-hydroxypyridine¹² and, to an even greater degree, in 2-hydroxypyrimidine.¹³ The closed H-bonded structures, $N\cdots H-O\cdots H-O$ and $N\cdots H-O\cdots H-N$, of the water complexes with the hydroxy and hydroxyamino tautomers, and the closed structures, $N-H\cdots O-H\cdots O=C$, for the oxo tautomers of the 2-hydroxypyridine and 2-pyrimidine basis with vicinal sites, are suitable structures to study the H-bond cooperativity effects.¹⁴ Also worth mentioning is that for 4-aminopyrimidine \cdot water, the most stable complex found was the closed structure $N\cdots H-O\cdots H-NH$.³

Detailed comparison of the experimental spectral results obtained for the isolated complexes with the *ab initio* predicted (scaled) frequencies and intensities has allowed us to develop some useful correlations.^{3,4,15} Among these correlations, the procedure for scaling the calculated frequencies of the H-bonded water modes to match the experimental frequencies has been developed for the $N\cdots HO-H$ -type complexes. This correction procedure is used and further elaborated in the present report. Furthermore, a similar method for scaling of the *ab initio* predicted frequencies of the modes of bonded water in the $C=O\cdots HO-H$ complexes is proposed and used to assist the assignment of the FT-IR spectra. Finally, the *ab initio* calculated interaction energies of different water complexes of TMC corrected for the basis set superposition error (BSSE) are compared with the relative concentration of these complex species in the inert matrix.

Lastly, we will demonstrate that the interplay between experimental and theoretical results can become more complicated, particularly if some factors present in the experiment are absent in the calculated model: we will show that it is possible to use not only the agreement but also the discrepancies between the experimental and theoretical data to aid the analysis of the

experimental spectra. We will describe instances where the calculated data, such as vibrational frequencies and Mulliken population analysis, can be used to support the idea that slightly different H-bonded structures are observed in the Ar matrix from those obtained from *ab initio* geometry calculations which do not include spectator argon atoms in the structures.

Methodology

Experimental Method. A detailed description of the experimental method used here has been presented elsewhere.^{1,16,17} Optimal sublimation temperatures were 40 and 30 °C for MOP and TMC, respectively, at the Ar deposition rate of about 5 mmol/h. Similar to all our earlier studies on water complexes in Ar,^{1-4,7} the water-to-base ratio varying between 1:1 and 1:5 was used. The latter ratio ensures excess amount of the 1:1 complex species to be present in the matrix with still weak spectral manifestations of higher-stoichiometry complexes.

MOP was prepared by methylation of the parent compound 2-pyrimidone using the method described by Curd and Richardson.¹⁸ 2-Pyrimidone was dissolved in basic, ethanolic solution and methyl iodide was added. After completion of the reaction, the methylated compound was recrystallized from ethanol solution. For the synthesis of TMC, 4-methoxy-1-methyl-2-pyrimidone, which was obtained from 2,4-dimethoxypyrimidine and methyl iodide,¹⁹ was dissolved in ethanol and this solution was saturated with dimethylamine at 0 °C.²⁰ After saturation the sealed flask was heated for 8 h at 150 °C and TMC precipitated on cooling. The compound was recrystallized from ethanol solution. The purity of both synthesized products was checked with NMR, mass spectrometry, and IR spectroscopy and they appeared to be more than 99% pure. 2-Pyrimidone \cdot HCl and methyl iodide were commercially available from JANSSEN Chimica, while 2,4-dimethoxypyrimidine was obtained from SIGMA. Twice distilled water was used for the water-doped samples, while Ar gas (99.9999%) from Air Liquide was used in all experiments.

Theoretical Method. Optimized geometries of free MOP and TMC were first determined at RHF/6-31++G** level. For MOP we also performed the geometry calculations at the MP2/6-31G** and MP2/6-31++G** levels. Augmentation of the split valence 6-31G basis set with polarization and diffuse functions on both hydrogen and second row atoms yields a basis set which possesses sufficient diffuseness and angular flexibility to describe reasonably well weak H-bonding interactions. Switching from the RHF to MP2 level of theory allowed us to account for the dispersion contribution to the intermolecular interaction energy, in addition to more accurately accounting for the electrostatic exchange, induction, and charge transfer interaction contributions. The IR frequencies, intensities, and the zero-point vibrational energy (ZPE) were subsequently computed using the analytical derivative procedure incorporated in the GAUSSIAN 92 program.²¹ Following these calculations, the total energies of the optimized structures were calculated at the MP2+0.9ZPE level (for ZPE determined with the RHF procedure) using the same basis set. Calculated RHF frequencies were scaled down by the single scaling factor 0.9 to approximately correct for vibrational anharmonicity, as well as for overestimation of the force constants at the RHF level. For the MP2 frequencies, two scaling procedures were used. In the first procedure, a single scaling factor of 0.96 was employed, and in the second procedure, two different scaling factors were used, 0.96 for all the modes except for the out-of-plane vibrations where the scaling factors was 1.00. In determining the H-bond energies, the basis set superposition error was corrected for by recalculating the monomer energies in the basis set of the heterodimers (counterpoise correction).

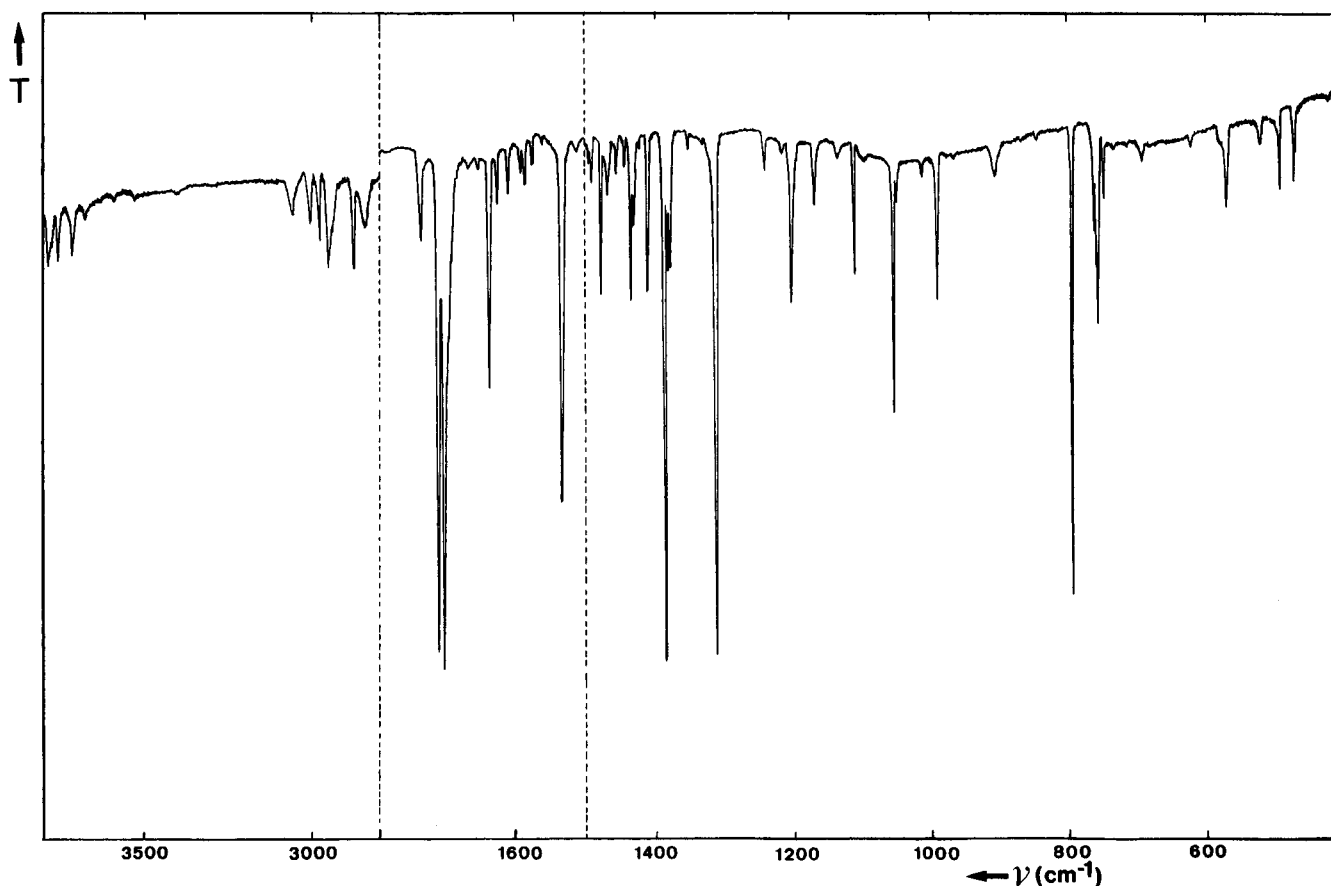


Figure 1. FT-IR spectrum of 1-CH₃-2-pyrimidone in Ar at 12 K (for sake of clarity, different ordinate expansions are used for different spectral regions).

The dispersion forces are expected to noticeably contribute to the stability of a H-bonded complex, and in order to account for this effect in the geometry optimization of the complex structure, a correlated method such as MP2 should be used.^{22,23} However, due to the size of the systems considered, such calculations would require very long computational time. Therefore, in our previous studies we have resorted to geometry optimizations at the RHF level of theory.^{1-4,7} In the present work, however, since there has been a disagreement between the RHF-optimized MOP·H₂O complex and the experimentally observed structure, we have also performed the geometry optimization of MOP and its water complexes at the MP2/6-31++G** level, and have subsequently carried out single-point energy calculations at the MP2/6-311++G**/MP2/6-31++G** level of theory. However, due to disk space limitations and limited computer time allotment, the frequency calculations were not possible at the MP2/6-31++G** level and all the structures were reoptimized at MP2/6-31G** level of theory and were followed by numerical MP2/6-31G** frequency calculations.

In the analysis of the experimental data, we argue that the interaction between the water-base complex and the argon atoms in the matrix cannot be neglected. In support of this argument, some additional calculations were performed concerning interaction the methylformamide complex with water and a single argon atom. This system was chosen because its H-bonding interaction with water resembles the interaction which exists in the MOP·H₂O complex. The structure of the complex was optimized at the MP2/6-31++G** level of theory and followed by frequency calculations at the same level.

Results and Discussion

We will first analyze the FT-IR monomer spectra of MOP and TMC in Ar in order to assign the vibrational modes, which

are expected to be sensitive to the H-bonding interactions with water. In the next step, these data will serve as the reference for the analysis of the spectral perturbations caused by H-bonding of the compounds to water molecules. Monomer spectra and frequencies of H₂O/Ar were presented in the first report of the series.¹

MOP/Ar. As far as we know, matrix spectral data for MOP have not yet been published in the literature. On the other hand, IR spectra of this compound have been obtained earlier in KBr dispersion and in dichloroethane solution.²⁴ Figure 1 illustrates the FT-IR spectrum of MOP, and Table 1 summarizes the vibrational assignments based on the detailed comparison with the *ab initio* calculated spectral parameters. In the upper frequency region, which is shown in the ordinate-expanded mode, weak absorptions due to different CH₃ stretches are observed. The important H-bond-sensitive mode $\nu_{C=O}$ is found as an intense doublet absorption at 1712/1704 cm⁻¹. The mean frequency of this doublet is somewhat smaller than the $\nu_{C=O}$ values in related compounds, *e.g.*, in 2-pyridone (1728 cm⁻¹)¹² or 4-pyrimidone (1725 cm⁻¹).¹³ A similar effect of frequency decrease induced by a vicinal methyl substitution was also observed in uracils.²⁵ The split of the $\nu_{C=O}$ spectral pattern is often observed for the carbonyl vibration and it is attributed to the Fermi resonance.²⁶ The bands observed at 1636 and 1530 cm⁻¹ are assigned to ring stretches with a large N₃C₄ stretching PED (potential energy distribution) contribution which makes them good tools for investigating H bonding at the N₃ atom. Many of the absorptions in the region 1500–1000 cm⁻¹ are easily assigned to methyl deformations and rockings, but only very small perturbations are expected for these vibrations from H bonding. Other H-bond-sensitive modes with considerable contributions from either ring stretchings or from $\gamma_{C=O}$ and $\delta_{C=O}$, are found at 1106 cm⁻¹ ($\nu(C_2N_3)$), 991 cm⁻¹ ($\nu(C_4C_5)$),

TABLE 1: Experimental (Ar Matrix) and Calculated (SCF/6-31++G) IR Spectral Data for 1-Methyl-2-pyrimidone**

experimental		calculated		PED ^c
ν (cm ⁻¹)	I^a (km·mol ⁻¹)	ν^b (cm ⁻¹)	I (km·mol ⁻¹)	
<i>d</i>		3074	2	$\nu(\text{C}_5\text{H})$ (88)
<i>d</i>		3046	4	$\nu(\text{C}_6\text{H})$ (89)
3003	14	2996	30	$\nu(\text{C}_4\text{H})$ (99)
2983	14	2981	14	$\nu^{\text{d}}_1(\text{CH}_3)$ (94)
2962	26	2981	12	$\nu^{\text{d}}_2(\text{CH}_3)$ (99)
2883	13	2903	40	$\nu^{\text{s}}(\text{CH}_3)$ (95)
1712/1704 ^e	1400	1739	971	$\nu(\text{C}_2\text{O})$ (78)
1636	167	1666	141	$\nu(\text{N}_3\text{C}_4)$ (36) + $\nu(\text{C}_5\text{C}_6)$ (23)
1530	407	1544	407	$\nu(\text{C}_5\text{C}_6)$ (23) + $\nu(\text{N}_3\text{C}_4)$ (21) + $\nu(\text{C}_4\text{C}_5)$ (13)
1479	24	1479	57	$\delta^{\text{d}}_1(\text{CH}_3)$ (45) + $\delta^{\text{s}}(\text{CH}_3)$ (12)
1456	11	1461	2	$\delta^{\text{d}}_1(\text{CH}_3)$ (38) + $\delta(\text{C}_5\text{H})$ (16) + $\delta^{\text{s}}(\text{CH}_3)$ (12)
1435	49	1439	7	$\delta^{\text{d}}_2(\text{CH}_3)$ (92)
1414	28	1422	21	$\delta^{\text{s}}(\text{CH}_3)$ (75)
1386/1382	102	1386	72	$\delta(\text{C}_4\text{H})$ (54)
1314	171	1303	91	$\delta(\text{C}_6\text{H})$ (24) + $\nu(\text{N}_1\text{C}_6)$ (17)
1200	24	1200	20	$\delta(\text{C}_6\text{H})$ (32) + $\nu(\text{N}_1\text{C}_2)$ (19) + $\nu(\text{C}_5\text{C}_6)$ (16)
1165	10	1159	10	$\delta(\text{C}_5\text{H})$ (40) + $\delta(\text{C}_6\text{H})$ (24)
1132	6	1127	2	$\rho_1(\text{CH}_3)$ (89)
1106	20	1107	11	$\nu(\text{C}_2\text{N}_3)$ (27) + (C_5C_6) (13) + $\delta_{\text{R}1}$ (12)
1051	49	1044	28	$\rho_2(\text{CH}_3)$ (34) + $\delta_{\text{R}1}$ (16) + $\nu(\text{C}_6\text{N}_1)$ (15) + $\delta(\text{C}_5\text{H})$ (15)
<i>d</i>		1012	0	$\gamma(\text{C}_4\text{H})$ (85) + $\gamma(\text{C}_6\text{H})$ (20)
<i>d</i>		990	0	$\gamma(\text{C}_6\text{H})$ (74) + $\gamma(\text{C}_5\text{H})$ (24)
991	19	973	27	$\nu(\text{C}_4\text{C}_5)$ (59) + $\nu(\text{N}_1\text{C}_2)$ (14)
902	11	893	20	$\delta_{\text{R}1}$ (49) + $\delta(\text{C}_2\text{N}_3)$ (16) + $\nu(\text{N}_1\text{C}_{11})$ (13)
793	38	804	52	$\gamma(\text{C}_2\text{O})$ (79) + $\tau_{\text{R}1}$ (23)
762/758/756	35	752	52	$\gamma(\text{C}_5\text{H})$ (80)
748	8	742	4	$\nu(\text{N}_1\text{C}_2)$ (29) + $\nu(\text{N}_1\text{C}_{11})$ (20) + $\nu(\text{C}_2\text{N}_3)$ (13) + $\nu(\text{C}_6\text{N}_1)$ (13)
<i>d</i>		592	0	$\delta_{\text{R}3}$ (44) + $\delta(\text{C}_2\text{O})$ (19) + $\delta_{\text{R}2}$ (17)
569	24	560	6	$\delta(\text{C}_2\text{O})$ (28) + $\delta_{\text{R}3}$ (33)
506 or 493	9 or 14	511	7	$\tau_{\text{R}1}$ (67) + $\gamma(\text{C}_2\text{O})$ (19) + $\tau_{\text{R}3}$ (18)
473	15	488	7	$\delta_{\text{R}2}$ (49) + $\delta(\text{C}_2\text{H})$ (16) + $\nu(\text{N}_1\text{C}_6)$ (12)
<i>f</i>		395	1	$\tau_{\text{R}3}$ (81) + $\gamma(\text{N}_1\text{C}_{11})$ (13)
<i>f</i>		335	6	$\delta(\text{N}_1\text{C}_{11})$ (70) + $\delta(\text{C}_2\text{O})$ (14)
<i>f</i>		209	1	$\gamma(\text{N}_1\text{C}_{11})$ (71) + τ_{R} (20) + $\tau(\text{CH}_3)$ (16)
<i>f</i>		132	1	$\tau(\text{CH}_3)$ (51) + $\tau_{\text{R}3}$ (26) + $\gamma(\text{N}_1\text{C}_{11})$ (22)
<i>f</i>		104	0	$\tau_{\text{R}3}$ (61) + $\tau(\text{CH}_3)$ (32) + $\tau_{\text{R}1}$ (17)

^a Experimental intensities normalized to the calculated intensity of the 1530 cm⁻¹ band (407 km/mol). ^b Uniform scaling factor 0.9. ^c Only contributions > 10 are listed: ν designates stretching, δ in-plane bending, γ out-of-plane deformation, ρ rocking and τ torsion mode; subscript R = ring mode; CH₃ stretches and in-plane deformations are further indicated by superscripts “d” (degenerate) and “s” (symmetric). ^d Too weak to be observed. ^e Strongest component of multiplet underlined. ^f Situated below studied region (< 400 cm⁻¹).

793 cm⁻¹ ($\gamma(\text{C}_2=\text{O})$), 748 cm⁻¹ ($\nu(\text{N}_1\text{C}_2)$), and 569 cm⁻¹ ($\delta(\text{C}_2=\text{O})$). The mean deviation between the experimental and the scaled *ab initio* RHF frequencies is 9.8 cm⁻¹, which is somewhat better than the deviations found for other model molecules studied earlier, e.g., pyridine¹ (13.0 cm⁻¹), pyrimidine¹ (11.2 cm⁻¹), 4-aminopyridine³ (14.4 cm⁻¹), 4-aminopyrimidine³ (16.0 cm⁻¹), 3-hydroxypyridine⁴ (15.0 cm⁻¹), and 4-hydroxypyridine⁴ (9.7 cm⁻¹). Similar to earlier observations, the experimental intensities agree rather well with the predicted ones, with some stronger deviations being observed only for a few modes. It may be concluded that very little doubt remains about the assignment of the H-bond-sensitive modes, $\nu_{\text{C}=\text{O}}$, $\gamma_{\text{C}=\text{O}}$, $\delta_{\text{C}=\text{O}}$, and $\nu(\text{N}_3\text{C}_4)$. Interestingly, for these modes the MP2/6-31G** frequencies seem to less accurately reproduce the experimental data than the RHF/6-31++G** frequencies. The mean deviation between the MP2 and experimental frequencies is 40 cm⁻¹, when one scaling factor is used, and 25 cm⁻¹, when three different scaling factors are used (see Methodology section). This is consistent with our previous observations.

TMC/Ar. Figure 2 shows the FT-IR spectrum of TMC in Ar. Table 2 presents the assignment which is proposed by comparison with the *ab initio* RHF/6-31++G** predicted frequencies and intensities. Again, our main interest is the assignment of the H-bond-sensitive modes. The $\nu_{\text{C}=\text{O}}$ mode is assigned to the doublet absorption observed at 1695/1685 cm⁻¹. The corresponding out-of-plane and in-plane bending modes

of the C=O group are assigned to the bands found at 781 and 613 cm⁻¹, respectively. All these frequencies are close to the corresponding values in MOP. Ring stretches with sizable PED contribution from the N₃C₄ bond vibration are assigned to the bands at 1639 and 1513 cm⁻¹. These values are also close to the corresponding frequencies in MOP. The mean deviation between the experimental and scaled *ab initio* frequencies is 9.1 cm⁻¹, which is slightly better than for MOP. Deviations between the experimental and predicted intensities are only more significant for the CH₃ modes, one ring in-plane bend, and the torsion mode predicted at 423 cm⁻¹. All these observations indicate that the proposed assignments, especially those of the H-bond-sensitive modes, are most probably correct.

MOP/H₂O/Ar. (A) Theoretical Results. Since MOP possesses two vicinal proton-acceptor sites, N₃ and C₂=O, formation of closed H-bonded complexes with two H bonds cannot be excluded. Table 3 summarizes our *ab initio* energy calculations for the MOP monomer and its two *ab initio* predicted stable complexes with water at the RHF and the MP2 levels of theory. The first question, which we intend to answer with the theoretical calculations, was whether the two closely located proton-acceptor sites result in formation of a single water complex or a pair of distinct complexes in which the two hydrogen bonds differ in strength and in length. Depending on the level of theory, two minima (RHF/6-31++G** and MP2/6-31++G**) or just one minimum (MP2/6-31G**) were found on the MOP-water PES. At the highest level of theory (MP2/

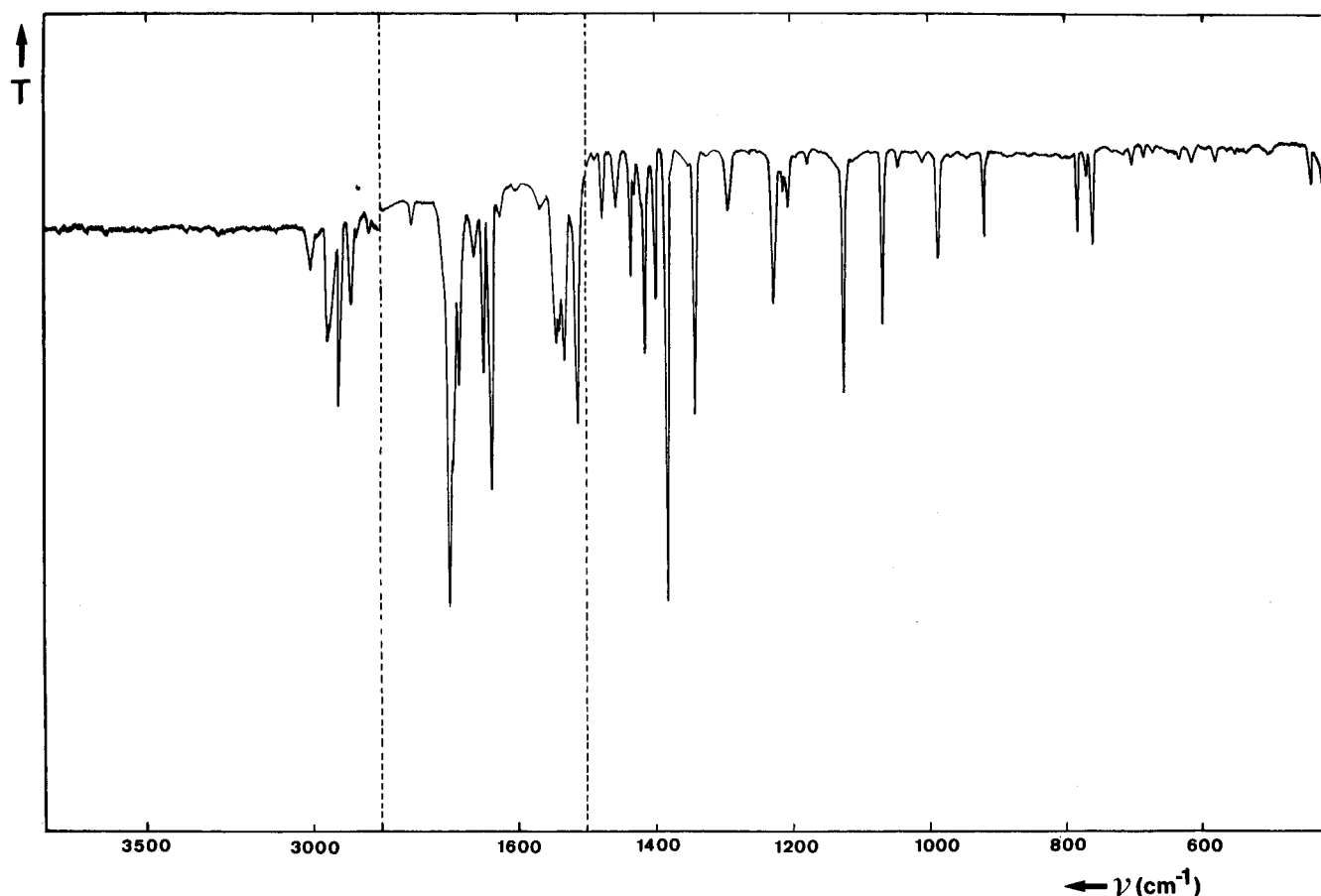


Figure 2. FT-IR spectrum of *N,N,1*-trimethylcytosine in Ar at 12 K (for sake of clarity, different ordinate expansions are used for different spectral regions).

6-31++G**) applied in the present calculations, the differences in the H-bond distances in the two complexes are large enough to conclude that, despite the resemblance in structures and small differences in total energies, the two geometries represent distinct complexes. As we demonstrated in the comparative study on the interaction of imidazole with water, the diffuse functions in the basis set and accounting for the electron correlation effects in the calculations are necessary to properly describe the H-bond interaction and to obtain reliable frequency shifts for those vibrations directly influenced by the H-bond interaction.^{23,27} This is consistent with the known nature of the H bond, which comprises dipole–dipole electrostatic interaction, induction exchange and dispersion interactions, and some charge transfer interaction. The MP2 level of theory accounts for the majority of the dispersion contribution and should also more correctly than the RHF level describe the other contributions for complexes where the RHF wave function represents reasonably well the state of the system. Additional diffuse sp shells in the 6-31++G** basis set should lead to a much better description of the σ -type interaction of the H bond and to a better accounting for the charge transfer effect.

First, we will describe in more detail the RHF results, because those can be directly compared with our previous RHF/6-31++G** results obtained for several model molecules and their water complexes modeling water interaction with cytosines and isocytosines and described in this series of papers.^{1–4}

The differences in the two geometries and the energies of the two MOP•water complexes (see Scheme 1 and Table 4) obtained at both RHF and MP2 levels of theory are very small. The first important result is that the H-bonding interactions of water at the N₃ atom and at the C₂=O group are comparable in strength at both the MP2/6-31++G**//RHF/6-31++G** and

MP2/6-311++G**//MP2/6-31++G** levels. As a matter of fact, the relative H-bond interaction energy difference between the two complexes is only 1.2 kJ•mol^{−1} at MP2/BSSE//RHF level. The second important result can be derived from the RHF- and MP2-optimized geometries of the two complexes. It is clear from the obtained geometries that in the N₃...HO–H complex a weak interaction exists between the second water H atom and the lone pair of O₇, and a similar weak interaction also exists in the C₂=O...HO–H complex between the second water H atom and the N₃ atom. The N₃...H₁₅ distance in the N₃...HO–H complex is 2.18 Å, and the O₇...H₁₇ distance is 2.43 Å, whereas the O₇...H₁₅ distance in the C₂=O...HO–H complex is 2.12 Å and the N₃...H₁₇ distance is 2.45 Å. Furthermore, the *r*_{OH} distances of both water OH bonds are not largely different, but both increased from the value in free water (0.943 Å) to 0.946 and 0.945 Å (complex with the stronger H bond at N₃) and to 0.947 and 0.944 Å (complex with the stronger H bond at C₂=O) at the RHF level. The formation of the second, weaker H bond explains why the RHF H-bond interaction energy in both MOP complexes are larger than for the N₁...HO–H complex of 4-aminopyridine (21.24 kJ•mol^{−1})^{3,27} in spite of a greater proton affinity (PA) value of the latter base (962 kJ•mol^{−1})²⁸ compared to MOP (estimated PA value 880–900 kJ•mol^{−1}; see further). We can anticipate that the primary H-bond interaction is somewhat weakened due to the additional interaction of the bonded water molecule with the second lone pair, either at O₇ or N₃. This so-called anticooperativity effect appears because the same water molecule acts simultaneously as a proton donor for two H bonds.²⁹ This H-bond weakening effect can be demonstrated by the comparison of the (primary) H-bond distances at RHF level in the N₃...HO (2.31 Å) and C₂=O...HO (2.18 Å) complexes of MOP with the correspond-

TABLE 2: Experimental (Ar Matrix) and Calculated (SCF/6-31++G) IR Spectral Data for 1,8,8-Trimethylcytosine**

experimental		calculated		PED ^c
ν (cm ⁻¹)	I^a (km·mol ⁻¹)	ν^b (cm ⁻¹)	I (km·mol ⁻¹)	
<i>d</i>		3097	1	$\nu(\text{C}_5\text{H})$ (97)
3008	2	3043	7	$\nu(\text{C}_6\text{H})$ (96)
<i>d</i>		3022	1	$\nu^{\text{d}}_1(\text{CH}_3)$ at C ₁₅ (111)
2958		2975	16	$\nu^{\text{d}}_2(\text{CH}_3)$ at C ₁₀ (100)
2951	21	2973	18	$\nu^{\text{d}}_1(\text{CH}_3)$ at C ₁₀ (91)
2948		2970	31	$\nu^{\text{d}}_1(\text{CH}_3)$ at C ₁₆ (110)
2924	25	2921	53	$\nu^{\text{d}}_2(\text{CH}_3)$ at C ₁₅ (86) + $\nu^{\text{s}}(\text{CH}_3)$ at C ₁₅ (15)
2921		2918	34	$\nu^{\text{d}}_2(\text{CH}_3)$ at C ₁₆ (92)
2890	13	2898	54	$\nu^{\text{s}}(\text{CH}_3)$ at C ₁₀ (92)
2871	13	2862	76	$\nu^{\text{s}}(\text{CH}_3)$ at C ₁₆ (73) + $\nu^{\text{s}}(\text{CH}_3)$ at C ₁₅ (28)
2858	2	2856	65	$\nu^{\text{s}}(\text{CH}_3)$ at C ₁₅ (69) + $\nu^{\text{s}}(\text{CH}_3)$ at C ₁₆ (31)
1698/1685 ^e	667	1721	1006	$\nu(\text{C}_2\text{O})$ (75)
1650/1639	351	1648	694	$\nu(\text{C}_5\text{C}_6)$ (38) + $\nu(\text{N}_3\text{C}_4)$ (14) + $\delta(\text{C}_6\text{H})$ (14)
1541/1530	316	1521	316	$\nu(\text{C}_4\text{C}_5)$ (17) + $\nu(\text{C}_4\text{N})$ (14) + $\delta(\text{C}_5\text{H})$ (13) + $\nu(\text{C}_6\text{N}_1)$ (12)
1513	183	1515	402	$\nu(\text{N}_3\text{C}_4)$ (25) + $\nu(\text{C}_4\text{N})$ (12)
		1482	15	$\delta^{\text{d}}_1(\text{CH}_3)$ at C ₁₆ (68)
1476	19	1472	7	$\delta^{\text{d}}_1(\text{CH}_3)$ at C ₁₀ (65) + $\delta^{\text{d}}_2(\text{CH}_3)$ at C ₁₅ (12)
		1471	8	$\delta^{\text{d}}_2(\text{CH}_3)$ at C ₁₅ (36) + $\delta^{\text{d}}_2(\text{CH}_3)$ at C ₁₆ (12) + $\delta^{\text{d}}_1(\text{CH}_3)$ at C ₁₅ (19)
1458	19	1462	11	$\delta^{\text{d}}_2(\text{CH}_3)$ at C ₁₆ (79)
1455		1458	12	$\delta^{\text{d}}_1(\text{CH}_3)$ at C ₁₅ (53) + $\delta^{\text{d}}_2(\text{CH}_3)$ at C ₁₅ (27)
1435	16	1447	33	$\delta^{\text{s}}(\text{CH}_3)$ at C ₁₆ (46) + $\delta^{\text{s}}(\text{CH}_3)$ at C ₁₀ (25)
1430		1439	7	$\delta^{\text{d}}_2(\text{CH}_3)$ at C ₁₀ (92)
1415	35	1427	57	$\delta^{\text{s}}(\text{CH}_3)$ at C ₁₀ (56) + $\delta^{\text{s}}(\text{CH}_3)$ at C ₁₆ (26)
1400	35	1415	48	$\delta^{\text{s}}(\text{CH}_3)$ at C ₁₅ (78)
1384	173	1382	354	$\nu(\text{C}_4\text{N})$ (21)
1342	93	1337	150	$\delta(\text{C}_6\text{H})$ (26) + $\nu(\text{C}_6\text{N}_1)$ (12)
1294	28	1287	20	$\nu^{\text{a}}(\text{C}_{15}\text{N}_{14}\text{C}_{16})$ (17) + $\nu(\text{C}_2\text{N}_3)$ (14) + $\nu(\text{N}_3\text{C}_4)$ (14)
1227	63	1230	72	$\nu^{\text{a}}(\text{C}_{15}\text{N}_{14}\text{C}_{16})$ (22) + $\nu(\text{N}_1\text{C}_2)$ (15) + $\nu(\text{N}_1\text{C}_{10})$ (12) + $\nu(\text{C}_5\text{C}_6)$ (12)
1210/1206	13	1200	27	$\delta(\text{C}_5\text{H})$ (30) + $\nu(\text{N}_1\text{C}_{10})$ (20) + δ_{R1} (12)
1178	3	1180	1	$\delta(\text{C}_6\text{H})$ (22) + $\rho_1(\text{CH}_3)$ at C ₁₆ (15)
1138	2	1136	7	$\rho_2(\text{CH}_3)$ at C ₁₅ (51) + $\rho_2(\text{CH}_3)$ at C ₁₆ (29)
<i>d</i>		1127	2	$\rho_2(\text{CH}_3)$ at C ₁₀ (90)
1124	76	1116	128	$\nu(\text{C}_2\text{N}_3)$ (14) + $\rho_2(\text{CH}_3)$ at C ₁₆ (12) + $\rho_1(\text{CH}_3)$ at C ₁₅ (15)
1110	3	1100	6	$\rho_2(\text{CH}_3)$ at C ₁₆ (50) + $\rho_2(\text{CH}_3)$ at C ₁₅ (35)
1068	44	1058	39	$\rho_1(\text{CH}_3)$ at C ₁₆ (32) + $\nu^{\text{a}}(\text{C}_{15}\text{N}_{14}\text{C}_{16})$ (27) + $\rho_1(\text{CH}_3)$ at C ₁₅ (25)
1045	3	1041	4	$\rho_1(\text{CH}_3)$ at C ₁₀ (32) + $\nu(\text{C}_6\text{N}_1)$ (16) + δ_{R1} (12)
1002	3	997	1	$\gamma(\text{C}_6\text{H})$ (98) + $\gamma(\text{C}_5\text{H})$ (16)
987	35	979	19	$\nu(\text{C}_4\text{C}_5)$ (32) + $\nu(\text{N}_1\text{C}_2)$ (19)
919	14	907	12	$\nu^{\text{s}}(\text{C}_{15}\text{N}_{14}\text{C}_{16})$ (48) + δ_{R1} (23)
781	38	789	55	$\gamma(\text{C}_2\text{O})$ (83) + τ_{R1} (17)
758	70	770	45	$\gamma(\text{C}_4\text{N})$ (49) + $\gamma(\text{C}_5\text{H})$ (45)
769	5	754	3	$\nu(\text{N}_1\text{C}_{10})$ (26) + $\nu(\text{N}_1\text{C}_2)$ (22)
703	21	704	13	$\gamma(\text{C}_5\text{H})$ (40) + $\gamma(\text{C}_4\text{N})$ (25) + τ_{R1} (18)
682	7	692	4	$\nu^{\text{s}}(\text{C}_{15}\text{N}_{14}\text{C}_{16})$ (21) + δ_{R1} (14)
613	11	601	7	δ_{R3} (25) + $\delta(\text{C}_2\text{O})$ (18) + $\delta(\text{N}_1\text{C}_{10})$ (16) + $\gamma_3(\text{C}_4\text{N})$ (15)
580	9	570	5	δ_{R3} (45)
503 ?	5	497	4	$\delta(\text{C}_{15}\text{N}_{14}\text{C}_{16})$ (36) + δ_{R2} (25)
442	39	427	11	$\rho(\text{C}_{15}\text{N}_{14}\text{C}_{16})$ (36) + $\delta(\text{C}_2\text{O})$ (15)
425	16	423	2	τ_{R2} (56) + τ_{R1} (28)
<i>f</i>		352	1	δ_{R2} (25) + $\delta(\text{C}_{15}\text{N}_{14}\text{C}_{16})$ (39) + $\nu(\text{C}_4\text{N})$ (14)
<i>f</i>		331	7	$\delta(\text{N}_1\text{C}_{10})$ (62) + $\delta(\text{C}_2\text{O})$ (14)
<i>f</i>		264	5	$\gamma(\text{N}_1\text{C}_{10})$ (32) + wag (C ₁₅ N ₁₄ C ₁₆) (19) + τ_{R2} (14) + $\tau(\text{CH}_3)$ at C ₁₆ (20)
<i>f</i>		217	3	$\delta(\text{C}_4\text{N})$ (45) + $\rho(\text{C}_{15}\text{N}_{14}\text{C}_{16})$ (21)
<i>f</i>		197	1	$\gamma(\text{N}_1\text{C}_{10})$ (60) + wag (C ₁₅ N ₁₄ C ₁₆) (16)
<i>f</i>		175	2	τ_{R1} (30) + $\tau(\text{CH}_3)$ + C ₁₆ (17)
<i>f</i>		121	1	$\tau(\text{CH}_3)$ at C ₁₀ (45) + wag (C ₁₅ N ₁₄ C ₁₆) (19) + $\tau(\text{C}_{15}\text{N}_{14}\text{C}_{16})$ (15)
<i>f</i>		104	2	$\tau(\text{CH}_3)$ + C ₁₀ (44) + wag (C ₁₅ N ₁₄ C ₁₆) (17) + $\gamma(\text{N}_1\text{C}_{10})$ (13)
<i>f</i>		85	1	τ_{R3} (57) + $\tau(\text{CH}_3)$ at C ₁₆ (26)
<i>f</i>		67	8	$\tau(\text{C}_{15}\text{N}_{14}\text{C}_{16})$ (41) + τ_{R3} (36) + wag (C ₁₅ N ₁₄ C ₁₆) (13)
<i>f</i>		32	1	$\tau(\text{CH}_3)$ at C ₁₅ (76) + $\tau(\text{C}_{15}\text{N}_{14}\text{C}_{16})$ (14)

^a Experimental intensities normalized to the calculated intensity of the 1530 cm⁻¹ band (316 km/mol). ^{b-f} See Table 1.

ing H-bond distances in pyrimidine·H₂O (2.13 Å for N···HO, Table 5) and 4-pyrimidone·H₂O (1.95 Å for C=O···HO)¹³, respectively.

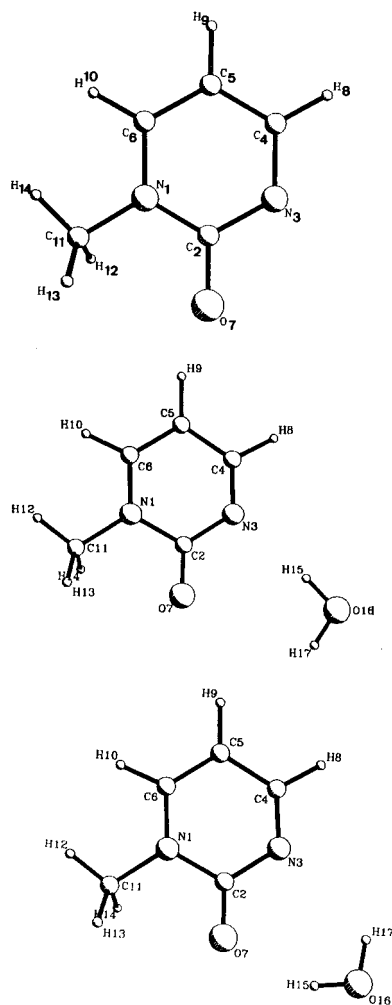
In the optimizations at MP2 level with the 6-31++G** basis set, the primary and secondary H-bonds in the two MOP·H₂O complexes decrease in length, in comparison with the RHF/6-31++G** results, by 0.07 to 0.23 Å due to accounting for the attractive dispersion effects, while the water OH distances increase by about 0.02 Å. With the 6-31G** basis set at the

MP2 level, when the geometry optimizations are started from the MP2/6-31++G* structures, both calculations converge to the same complex where the H-bond distances are 2.29 Å (N₃···H—O) and 2.20 Å (C₂=O···H—O), which seems to be an intermediate structure between the two structures obtained at the RHF and MP2 level with the 6-31++G** basis set. This result indicates that even if there are two minima on the MOP·water PES, they are very close to each other, and the barrier separating them is probably very low. It is, therefore, question-

TABLE 3: 1-Methyl-2-pyrimidone (MOP) and Its Complexes with Water. Total (au) and Relative (kJ·mol⁻¹) Energies Calculated with the 6-31++G (a) or the 6-311++G** (b) Basis Set^a**

	MOP	N ₃ ···HO-H		C=O···HO-H	
		6-31++G**	6-311++G**	6-31++G**	6-311++G**
SCF	-376.6148210	-452.6569962	-452.7457688	-452.6570206	-452.7456531
MP2 ^b	-377.7860194	-454.0321402	-454.2063307	-454.0320573	-454.2061933
SCF (base with ghost water orbitals)		-376.6150865		-376.6151002	
MP2 (base with ghost water orbitals)		-377.7868120		-377.7868356	
SCF (water with ghost base orbitals)		-76.0317692		-76.0318468	
MP2 (water with ghost base orbitals)		-76.2336532		-76.2340094	
ZPE ^c	0.1060479	0.12934809		0.1293376	
total	-377.6799715	-453.9027921	-454.0769826	-453.9027197	-454.0768557
ΔE ^d		0.0	0.0	0.19	0.33
H-bond energy (SCF/BSSE+ZPE)		-20.26		-19.91	
H-bond energy (MP2/BSSE+ZPE)		-24.09		-22.90	
μ (D)	6.65	9.54	10.03	9.84	10.29

^a All molecular geometries optimized at the SCF/6-31++G** (a) or the MP2/6-31++G** (b) level (Scheme 1). ^b Only valence correlation is considered. ^c Calculated at SCF/6-31++G** level as $0.9\sum h\nu_i/2$. ^d Energy difference between isomeric complexes.

SCHEME 1

able if they can be distinguished via IR spectrometry even at very cold temperatures.

Table 6 summarizes the *ab initio* (RHF) calculated frequencies for the MOP N₃···HO-H···O=C₂ and C₂=O···HO-H···N₃ complexes. We also present in Table 6 the PED analysis for the N₃···HO-H···O=C₂ complex. These PEDs and also the predicted frequency shifts are nearly the same for the majority of vibrations in both complexes (Table 6). However, clear differences in frequency perturbations are observed for $\nu_{C=O}$, $\gamma_{C=O}$, and $\delta_{C=O}$ (three different modes) which are noticeably stronger for the C₂=O···HO-H···N₃ species.

(B) Experiment. The proton affinities of the N₃ and O₇ sites in MOP are not known from experiment. However, the PA value of the O₇ site can be estimated with the use of the $\Delta\nu_{OH}/\Delta PA$ correlation established for H-bonded complexes of phenol with different C=O basis in inert solution.³⁰ Although X-ray diffraction and IR studies have revealed that protonation of MOP takes place at the N₃ atom,³¹ H bonding of MOP with phenol occurs only at the C₂=O site and this interaction is characterized by the thermodynamic parameters, $K = 15 \text{ dm}^3\cdot\text{mol}^{-1}$, $\Delta H = -25 \text{ kJ}\cdot\text{mol}^{-1}$, and $\Delta\nu_{OH} = 310 \text{ cm}^{-1}$.³² Using the above-mentioned correlation and the frequency shift measured in 1,2-dichloroethane, the PA value of $887 \text{ kJ}\cdot\text{mol}^{-1}$ is obtained for the MOP O₇ site. This value is close to the crudely estimated PA value of $892 \text{ kJ}\cdot\text{mol}^{-1}$ for the N₃ atom of MOP.³³

Figure 3 illustrates the high-frequency region of the FT-IR spectrum of MOP isolated in H₂O-doped Ar matrices. Prominent changes with respect to the spectrum of H₂O/Ar¹ are observed at $3493/3487$ and 3453 cm^{-1} (water ν_1 region), and at 3705 and 3703 cm^{-1} (water ν_3 region). For the sake of clarity, a more expanded spectrum in this spectral region is shown in Figure 4. The new absorptions manifest the presence of at least two different types of H-bonded complexes of MOP with water. Using the estimated PA value of MOP at the O₇ site from the vibration-correlation diagram, we can assign the doublet band at $3493/3487$ to the open C₂=O···HO-H complex species. The fact that this complex band has the frequency in the expected narrow spectral range demonstrates that the open C₂=O···HO-H complex rather than a closed complex occurs in the Ar matrix. The other complex ν_{OH} band at 3453 cm^{-1} is then assigned to the other open complex, N₃···HO-H, in view of a slightly greater PA value of N₃ compared to O₇, and in view of the anticipated larger frequency shifts resulting from more significant charge transfer in the N···HO-H complex.³³ The estimated PA values of the two MOP interaction sites in the range of $880\text{--}900 \text{ kJ}\cdot\text{mol}^{-1}$ are relatively close to the corresponding PA values at the C₄=O interaction site in uracil ($870 \text{ kJ}\cdot\text{mol}^{-1}$) and at the N atom(s) in pyrimidine ($881 \text{ kJ}\cdot\text{mol}^{-1}$).²⁸ As a matter of fact, ν_{OH} absorptions for the open C=O···HO-H and N···HO-H complexes of these basis have been observed at 3513^{34} and 3468 cm^{-1} ,¹ respectively, which again supports our determination that only open H-bonded complexes of MOP exist in the low-temperature matrix. The slightly larger frequency shifts for the MOP complexes are consistent with greater PA values of both interaction sites in this methylated oxo base. Other characteristic absorptions manifesting the presence of the open C₂=O···HO-H complex are the ν_{OH} mode located at 3705 cm^{-1} , the frequency-decreased $\nu_{C=O}$ band at $1690 (-14) \text{ cm}^{-1}$, and the frequency-increased

TABLE 4: SCF/6-31++G and MP2/6-31++G** Geometries of 1-Methyl-2-pyrimidone (MOP) and SCF/6-31++G** Geometry of 1,8,8-Trimethylcytosine (TM)C and of Their H-Bonded Complexes with Water**

	MOP ^a	N ₃ ...HO ^a	N ₃ ...HO ^b	C=O...HO ^a	C=O...HO ^b	TMC ^a	N ₃ ...HO ^a	C=O...HO ^a	(Me ₂)N...HO ^a
Distances (Å)									
N ₁ C ₂	1.399	1.395	1.417	1.394	1.415	1.405	1.399	1.398	1.403
C ₂ N ₃	1.377	1.376	1.389	1.375	1.388	1.356	1.356	1.353	1.359
N ₃ C ₄	1.283	1.286	1.319	1.286	1.320	1.304	1.310	1.308	1.300
C ₄ C ₅	1.426	1.423	1.414	1.423	1.414	1.445	1.445	1.443	1.441
C ₅ C ₆	1.347	1.349	1.370	1.348	1.370	1.344	1.343	1.344	1.345
C ₆ N ₁	1.349	1.349	1.357	1.349	1.357	1.346	1.348	1.347	1.346
C ₂ O	1.198	1.200	1.235	1.203	1.237	1.203	1.206	1.209	1.202
C ₄ H	1.079	1.078	1.085	1.078	1.086				
C ₅ H	1.071	1.071	1.079	1.071	1.079	1.068	1.068	1.068	1.068
C ₆ H	1.074	1.074	1.082	1.074	1.082	1.074	1.074	1.074	1.074
N ₁ Me	1.460	1.461	1.464	1.461	1.464	1.456	1.458	1.458	1.457
C ₄ N						1.349	1.340	1.344	1.362
H _{15or23} ... ^c		2.308	2.179	2.181	2.116		2.178	2.033	2.291
H _{17or25} ... ^d		2.562	2.434	2.688	2.453		3.013	3.099	
OH (H ₂ O)	0.943	0.945 ^e	0.966 ^e	0.944 ^e	0.966 ^e	0.943	0.943 ^e	0.943 ^e	0.943 ^e
		0.946 ^f	0.969 ^f	0.947 ^f	0.969 ^f		0.949 ^f	0.950 ^f	0.946 ^f
Angles (deg)									
N ₁ C ₂ N ₃	117.38	117.52	117.1	117.72	117.35	117.84	118.19	118.42	117.70
C ₂ N ₃ C ₄	119.71	119.87	119.5	119.66	119.21	121.86	121.76	121.47	121.82
N ₃ C ₄ C ₅	124.73	124.41	124.4	124.52	124.56	121.53	121.20	121.48	121.74
C ₄ C ₅ C ₆	115.49	115.56	116.5	115.55	116.49	116.05	116.22	116.11	115.94
N ₁ C ₂ O ₇	119.02	119.30	119.0	119.01	118.79	117.98	118.42	117.85	118.31
N ₃ C ₂ O ₇	123.61	123.18	123.85	123.23	123.86	124.18	123.39	123.79	123.99
N ₃ C ₄ H ₈	116.22	116.29	115.68	116.27	115.66				
C ₅ C ₄ H ₈	119.05	119.30	119.90	119.21	119.79				
C ₄ C ₅ H ₉ (orH ₈)	122.29	122.26	122.24	122.27	122.26	123.59	123.35	123.45	123.77
C ₆ C ₅ H ₉ (orH ₈)	122.22	122.18	121.26	122.18	121.25	120.36	120.42	120.44	120.29
C ₅ C ₆ H ₁₀ (orH ₉)	122.69	122.61	123.49	122.67	123.55	121.38	121.39	121.47	121.37
C ₂ N ₁ C ₁₁ (orC ₁₀)	116.84	116.91	115.99	116.95	116.05	117.61	117.71	117.76	117.56
N ₃ C ₄ N ₁₄						118.57	118.12	118.15	117.85
C ₅ C ₄ N ₁₄						119.91	120.68	120.37	120.39
C ₄ N ₁₄ C ₁₅						120.45	118.92	119.31	118.65
C ₄ N ₁₄ C ₁₆						121.38	121.29	121.23	120.47
H...		7.72	8.17	9.11	9.30		0.66	5.08	4.16
HOH	107.09	103.59		103.64					

^a SCF/6-31+G**, ^b MP2/6-31++G**, ^c Primary H-bond interaction, ^d Secondary H-bond interaction, ^e "Free" OH group, ^f Bonded OH group.

TABLE 5: Survey of SCF/6-31++G Calculated Frequencies and H-Bond Distances, Proton Affinities PA_N, and Optimal Scaling Factors of the ν^b_{OH} (Water) Mode for Different B...H—OH Complexes^a**

molecule	proton affinity ²² (kJ/mol)	ν ^b _{OH} (cm ⁻¹)	ν ^f _{OH} (cm ⁻¹)	B...H distance (Å)	scaling factor for ν ^b _{OH}
water		4147	4269		0.877
water dimer ²⁷	697	4098	4243	2.040	0.872
pyrimidine ¹	881	4063	4237	2.135	0.854
3-hydroxypyridine ⁴	920	4047	4232	2.119	0.847
pyridine ¹	924	4038	4231	2.107	0.842
imidazole ²⁷	930	4031	4231	2.089	0.842
4-hydroxypyridine ⁴	937	4031	4231	2.094	0.835
4-aminopyridine ³	962	4017	4229	2.081	0.826
MOP N ₃ ...HO—H...O=C	892	4127	4219	2.308	0.870
MOP C=O...HO—H...N ₃	887	4123	4223	2.181	0.870
TMC N ₃ ...HO—H	930–960	4079	4224	2.178	0.843
TMC C=O...HO—H	930–960	4069	4230	2.033	0.852
TMC N ₁₄ ...HO—H	?	4118	4242	2.291	0.872

^a Geometries optimized at SCF/6-31++G** level.

γ_{C=O} mode at 797 (+4) cm⁻¹ (Figure 5). Figure 6 illustrates the FT-IR spectrum of the MOP/H₂O/CHCl₃ ternary solution at ambient temperature. Only one complex band is observed here in the 3600–3300 cm⁻¹ spectral region at 3455 cm⁻¹ which we attribute to the water ν^b_{OH} mode in the C₂=O...HO—H complex. The corrected frequency shift in solution is 158 cm⁻¹, which is somewhat smaller than the corrected shift in Ar (179 cm⁻¹). Apart from a low-frequency asymmetry of this complex band, there are no further spectral indications of a possible interaction at the N₃ site in solution, and the same result has been found for the H bonding of MOP with phenol.³¹ Preference of a particular H-bond interaction site at room temperature in solution in contrast to the low-temperature matrix, where other

sites can be preferred, is frequently observed and most probably originates from a stronger influence of the thermodynamic control on the complex stability at room temperature than at 12 K.³⁵

With some confidence we can conclude that the complex bands observed at 3453 and 3703 cm⁻¹ in the spectrum shown in Figures 3 and 4 originate from the open H-bond interaction at the N₃ atom. The latter ν^f_{OH} mode observed at a slightly lower frequency than that for the C₂=O...HO—H complex has also been found in pyrimidine·H₂O/Ar,¹ which supports its assignment to the N₃...HO—H complex. The frequency-increased ν(N₃C₄) band gives further conformation to the presence of this complex species. The observation of a doublet-

TABLE 6: Calculated (SCF/6-31++G) Spectral Data for the $N_3\cdots HO-H\cdots O=C_2$ and $C_2=O\cdots HO-H\cdots N_3$ H-Bonded Complexes of 1-Methyl-2-pyrimidone with Water**

N ₃ ⋯HO—H⋯O=C ₂		C ₂ =O⋯HO—H⋯N ₃		PED ^b
<i>ν</i> (cm ⁻¹) ^a	<i>I</i> (km/mol)	<i>ν</i> (cm ⁻¹) ^a	<i>I</i> (km/mol)	
Water Modes				
4219	111	4224	74	<i>ν</i> ⁱ (OH) (97)
4127	149	4123	145	<i>ν</i> ^b (OH) (96)
1786	223	1788	241	δ(HOH) (92)
545	231	555	211	N⋯HO o.o.p. wag (106) ^c
266	13	249	24	HO tors. about N⋯HO (90)
204	84	187	94	δ(N⋯HO) (74) + i.p. butterfly (18)
111	6	125	2	<i>ν</i> (N⋯OH) (95)
21	2	22	1	o.o.p. butterfly (88)
21	9	21	8	i.p. butterfly (72) + δ(N⋯HO) (20)
Base Modes				
3076 (+2)	1	3075 (+1)	1	<i>ν</i> (C ₅ H) (88)
3049 (+3)	3	3050 (+4)	3	<i>ν</i> (C ₆ H) (89)
3004 (+8)	22	3003 (+7)	24	<i>ν</i> (C ₄ H) (99)
2985 (+4)	12	2985 (+4)	12	<i>ν</i> ^d ₁ (CH ₃) (94)
2984 (+3)	10	2985 (+4)	10	<i>ν</i> ^d ₂ (CH ₃) (99)
2950 (+2)	36	2906 (+3)	36	<i>ν</i> ^s (CH ₃) (96)
1732 (−7)	874	1724 (−15)	934	<i>ν</i> (C=O) (74)
1663 (−3)	121	1662 (−4)	106	<i>ν</i> (N ₃ C ₄) (34) + <i>ν</i> (C ₅ C ₆) (23)
1554 (0)	551	1544 (0)	241	<i>ν</i> (C ₅ C ₆) (20) + <i>ν</i> (N ₃ C ₄) (19) + <i>ν</i> (C ₄ C ₅) (14)
1479 (0)	5	1479 (0)	5	δ ^d ₁ (CH ₃) (43) + δ ^s (CH ₃) (13)
1461 (0)	1	1461 (0)	1	δ ^d ₁ (CH ₃) (40) + δ(C ₅ H) (15)
1440 (+1)	8	1440 (+1)	8	δ ^d ₂ (CH ₃) (92)
1421 (−1)	30	1421 (−1)	29	δ ^s (CH ₃) (74)
1386 (0)	82	1386 (0)	80	δ(C ₄ H) (50)
1301 (−2)	105	1300 (−3)	102	δ(C ₆ H) (23) + <i>ν</i> (N ₁ C ₆) (16) + <i>ρ</i> ₁ (CH ₃) (14) + δ(C ₄ H) (13)
1201 (+1)	15	1202 (+2)	16	<i>ν</i> (N ₁ C ₁₁) (29) + <i>ν</i> (N ₁ C ₂) (21) + <i>ν</i> (C ₅ C ₆) (15)
1162 (+3)	8	1162 (+3)	7	δ(C ₅ H) (40) + δ(C ₆ H) (21)
1128 (+1)	2	1128 (+1)	2	<i>ρ</i> ₁ (CH ₃) (89)
1111 (+4)	9	1111 (+4)	9	<i>ν</i> (C ₂ N ₃) (26) + <i>ν</i> (C ₅ C ₆) (14) + δ _{R1} (12)
1046 (+2)	25	1046 (+2)	27	<i>ρ</i> ₂ (CH ₃) (33) + δ _{R1} (16) + <i>ν</i> (C ₆ N ₁) (14) + δ(C ₅ H) (15)
1015 (+3)	0	1014 (+2)	0	<i>γ</i> (C ₄ H) (85) + <i>γ</i> (C ₆ H) (20)
991 (+1)	0.2	991 (+1)	0.2	<i>γ</i> (C ₆ H) (74) + <i>γ</i> (C ₅ H) (24) + <i>γ</i> (C ₄ H) (16)
978 (+5)	33	978 (+5)	32	<i>ν</i> (C ₄ C ₅) (58) + <i>ν</i> (N ₁ C ₂) (15)
894 (+1)	21	895 (+2)	21	δ _{R1} (48) + <i>ν</i> (C ₂ N ₃) (16) + <i>ν</i> (N ₁ C ₁₁) (13)
804 (0)	60	806 (+2)	61	<i>γ</i> (C=O) (80) + <i>τ</i> _{R1} (22)
756 (+4)	53	757 (+5)	53	<i>γ</i> (C ₅ H) (80)
746 (+4)	4	746 (+4)	3	<i>ν</i> (N ₁ C ₂) (28) + <i>ν</i> (N ₁ C ₁₁) (21) + <i>ν</i> (C ₂ N ₃) (13) + <i>ν</i> (C ₆ N ₁) (13)
596 (+4)	0.2	596 (+4)	0.2	δ _{R3} (47) + δ(C=O) (17) + δ _(R2) (15)
563 (+3)	6	564 (+4)	7	δ(C=O) (31) + δ _{R3} (30)
511 (0)	3	514 (+3)	27	<i>τ</i> _{R1} (67) + <i>γ</i> (C=O) (16) + <i>τ</i> _{R2} (15)
490 (+2)	13	491 (+3)	9	δ _{R1} (48) + δ _{R2} (15) + <i>ν</i> (N ₁ C ₁₁) (12)
396 (+1)	10	398 (+3)	3	<i>τ</i> _{R2} (81) + <i>γ</i> (N ₁ C ₁₁) (15)
336 (+1)	8	340 (+5)	10	δ(N ₁ C ₁₁) (69) + δ _{R3} (14)
210 (+1)	5	208 (−1)	2	<i>γ</i> (N ₁ C ₁₁) (73) + <i>τ</i> _{R2} (20)
132 (0)	1	133 (+1)	2	<i>τ</i> (CH ₃) (56) + <i>τ</i> _{R3} (15) + <i>τ</i> _{R1} (15)
108 (+4)	0	108 (+4)	1	<i>τ</i> _{R3} (57) + <i>τ</i> _{R1} (16) + <i>τ</i> (CH ₃) (39)

^a Water modes unscaled, base modes scaled with uniform scaling factor 0.9. ^b PEDs for the $N_3\cdots HO-H\cdots O=C_2$ complex. ^c Description of intermolecular modes approximative in terms of the comparable modes for open complexes $N\cdots HO^3$.

splitted complex ν^b_{OH} band for the open $C_2=O\cdots HO-H$ species is consistent with many other similar observations in Ar matrices,^{4,25,36} and probably originates from two slightly different orientations of the bonded water molecule with respect to the base molecule in the open complex. In view of the noticeably smaller intensity of the complex band at 3453 cm⁻¹, it may be concluded that the concentration of the $N_3\cdots HO-H$ complex is definitely smaller than the concentration of the $C_2=O\cdots HO-H$ species. However, since the *ab initio* geometry optimization leads to complex structures with a second, weaker H bond in each of the complexes, we cannot directly compare this experimental intensity ratio for the open complexes with the *ab initio* predicted stability difference as it was done for the complexes of 4-aminopyridine³ or 3- and 4-hydroxypyridine⁴ with water.

(C) Differences between the Experimental and Theoretical Results. The experimental IR spectral analysis and the theoretical results obtained with the 6-31++G** basis set at the RHF

and MP2 levels identify slightly different structures for the MOP•water complexes. The spectral data indicate that in the Ar matrix the complexes have more open character than the most stable structures obtained in the *ab initio* calculations and that the second weaker H bond predicted by the calculations either does not exist, or is much weaker, or it is replaced in the matrix by the interaction with Ar atoms. This last possibility will be substantiated in the next section by the results of additional calculations on some model systems involving H bonding with water and interaction with argon atoms.

Table 5 demonstrates that the RHF predicted ν^b_{OH} frequency and H-bond distances of the nearly closed complexes are much larger than the corresponding values for the open pyrimidine•water complex at the N atom with about the same proton affinity. This indicates that the “closed” complexes, which are energetically the most stable, are characterized by noticeably smaller frequency shifts of the most strongly bonded water OH group. This is even better demonstrated by the differences

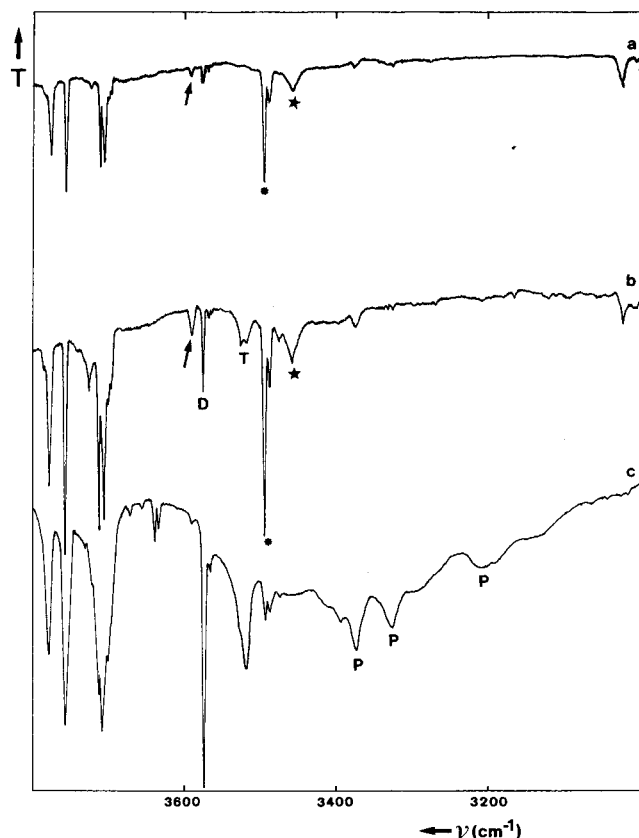


Figure 3. ν_3 – ν_1 (H₂O) and the ν_{OH} region of the FT-IR spectrum of 1-methyl-2-pyrimidone/H₂O/Ar at 12 K (a, H₂O/Ar = 1/500; b, H₂O/Ar = 1/200; c, H₂O/Ar = 1/100, annealed; *: C₂=O...HO–H complex; ★, N₃...HO–H complex; †, “closed” complexes; D, T, P = water dimer, trimer, polymer).

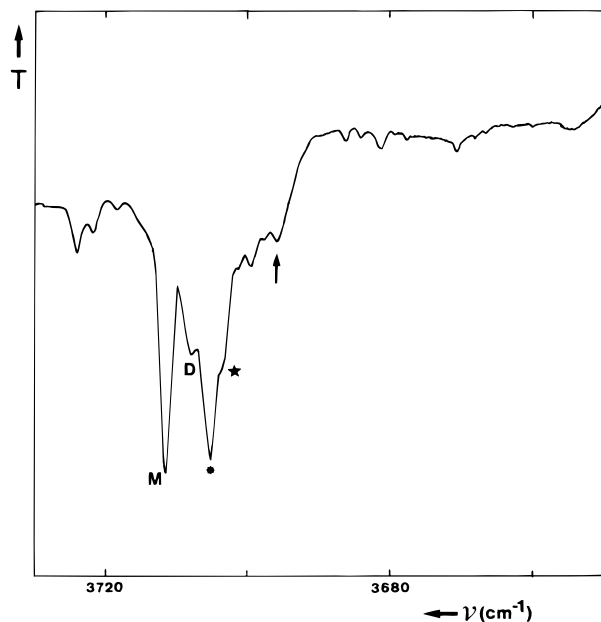


Figure 4. ν_3 (H₂O) region of the FT-IR spectrum of 1-methyl-2-pyrimidone/H₂O/Ar (H₂O/Ar = 1/500) at 12 K (M, D = water monomer, dimer; *, C₂=O...HO–H complex; ★, N₃...HO–H complex; †, “closed” complexes).

between the calculated Mulliken charges for the “closed” complexes and the free MOP base upon complexation. The negative charge on N₃ increases by 0.04 in \bar{e} units, while the positive charge on the H atom of water increases by 0.05. The charge increases at the same centers are much larger for the N...HO–H pyrimidine·water complex (0.08 \bar{e} and 0.08 \bar{e}),

which is consistent with larger frequency shifts in the latter complex. The presence of two different H bonds, *i.e.*, one somewhat weakened, but still a relatively strong one, and the weak one, gives rise to a ν_{OH}^b vibration with lower anharmonicity compared to an open complex with a single strong H bond. This can be determined based on the relation between the experimental frequency ν_{OH}^b and the scaling factor ν^{exp}/ν^{theor} which we have determined for several B...HO–H-type complexes.^{4,27} Comparison of the values of the scaling factors obtained before for some open complexes and results of Table 5 indicates that the ratio between the predicted and measured ν_{OH}^b frequencies for the nearly closed complexes are closer to 1 than for the open complexes. The calculated frequencies of the closed MOP·water complexes are not far from those in the water dimer, and thus the scaling factor in the range 0.880–0.870 may be expected for the bonded water stretching mode in these structures. Application of such a factor to the calculated frequencies leads to frequencies in the region of 3620–3580 cm^{-1} .

The rather large frequency difference between the ν_{OH}^b mode in the previously studied open N...HO–H and C=O...HO–H complexes and in the previously calculated nearly-closed N...HO–H...O=C and C=O...HO–H...N complexes undoubtedly results from the anticooperativity effect in the latter systems, which is also reflected by a large difference in the *ab initio* RHF-predicted H-bond distances in the MOP complex N...HO–H...O=C and in the open complex of pyrimidine with similar proton affinity.

We have a reason to believe that, since the frequency shifts of the water modes for the two MOP·water complexes observed in the Ar matrix follow the experimental correlations for the open N...H–OH and C=O...H–OH complexes (established previously), they must have a similar “open” structure as those determined for pyridine and pyrimidine N...H–OH H-bonded complexes with water.¹ The question arises why there is a difference between the *ab initio* predicted structures and the experimental matrix-isolated complexes. We can rephrase the question: Why is the second, weaker H bond not formed in the low-temperature matrix, where the formation of complexes should almost completely be governed by the interaction enthalpy. One possible explanation may be that the second, very weak H bond is replaced by a stronger interaction with the matrix material. This interaction by replacing the second, weaker H-bond interaction can allow water to strengthen its now single H-bond interaction with MOP, wherein reducing the anticooperativity effect. In this situation, the frequency shifts for the OH group engaged in the interaction with argon atoms are expected to be similar to the shift observed for water in Ar matrices. As we will demonstrate in the following section, the influence of the matrix material on the formation of the complex can explain the differences between experiment and theory, since this influence is not accounted for in the theoretical calculations.

(D) Involvement of Argon in the Formation of Anticooperative H Bonds in the Matrix. We first optimized the water·Ar complex at the MP2/6-311++G** level and obtained the interaction energy of 2.0 kJ/mol. At the MP4/6-311++G**//MP2/6-311++G** level, this value increased to 2.1 kJ/mol. With the use of the 6-31++G** basis set and the MP2 method, we obtained a slightly lower interaction energy of 1.7 kJ/mol. These values are very similar to the values reported in the review of Chalasinski and Szczesniak.²²

Next, additional calculations were carried out at the MP2/6-31++G** level of theory for methylformamide (MF) (see Scheme 2), which models the H-bonding interaction sites of MOP, for MF·water dimer and for its MF·water·Ar trimer.

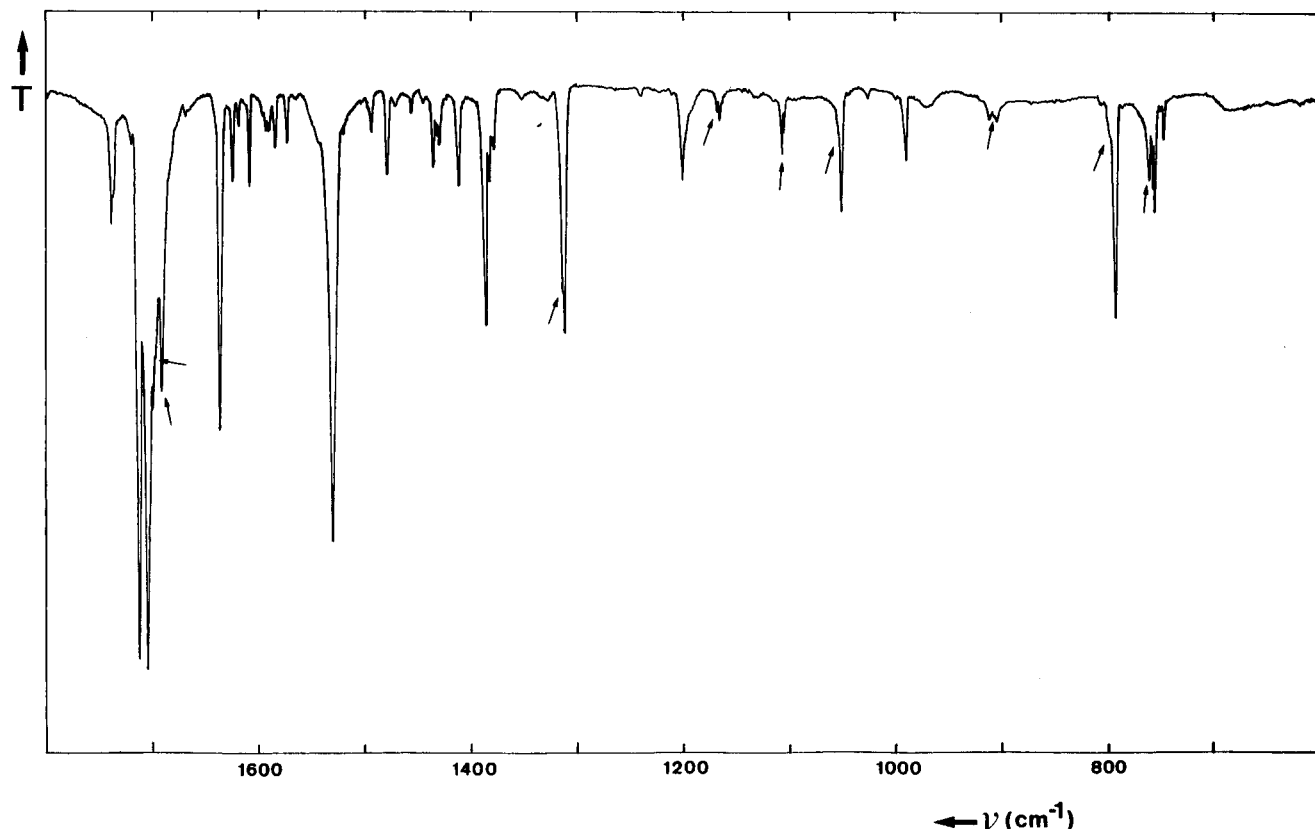


Figure 5. Perturbation of the base fundamentals in the FT-IR spectrum of 1-methyl-2-pyrimidone/H₂O/Ar (H₂O/Ar = 1/200) at 12 K (↑, shifted base mode).

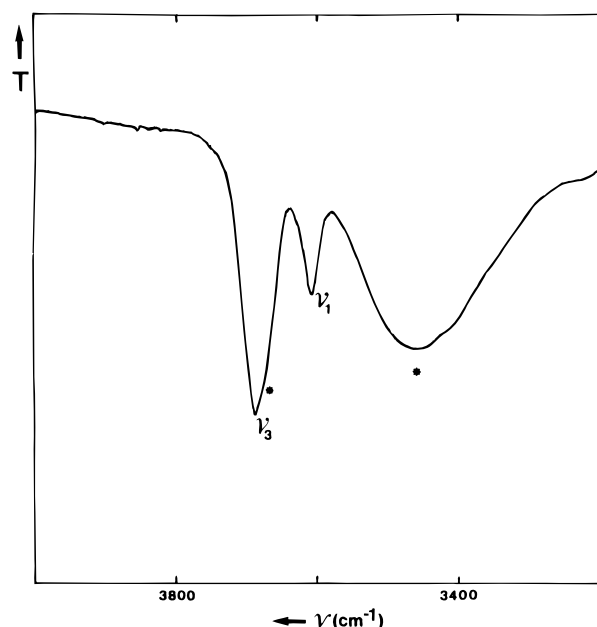


Figure 6. Water stretching region of the FT-IR spectrum of a ternary solution 1-methyl-2-pyrimidone/H₂O/CHCl₃ at room temperature ($C_{\text{base}} = 0.18 \text{ mol} \cdot \text{dm}^{-3}$; $C_{\text{water}} = 0.005 \text{ mol} \cdot \text{dm}^{-3}$; * = C₂=O...HO-H complex).

Geometry optimizations were followed by numerical frequency calculations. The purpose of these calculations was to determine the role of an argon atom which is put in contact with a dimer of a water molecule H-bonded to a molecule which has two closely-located, proton-accepting centers as in MOP.

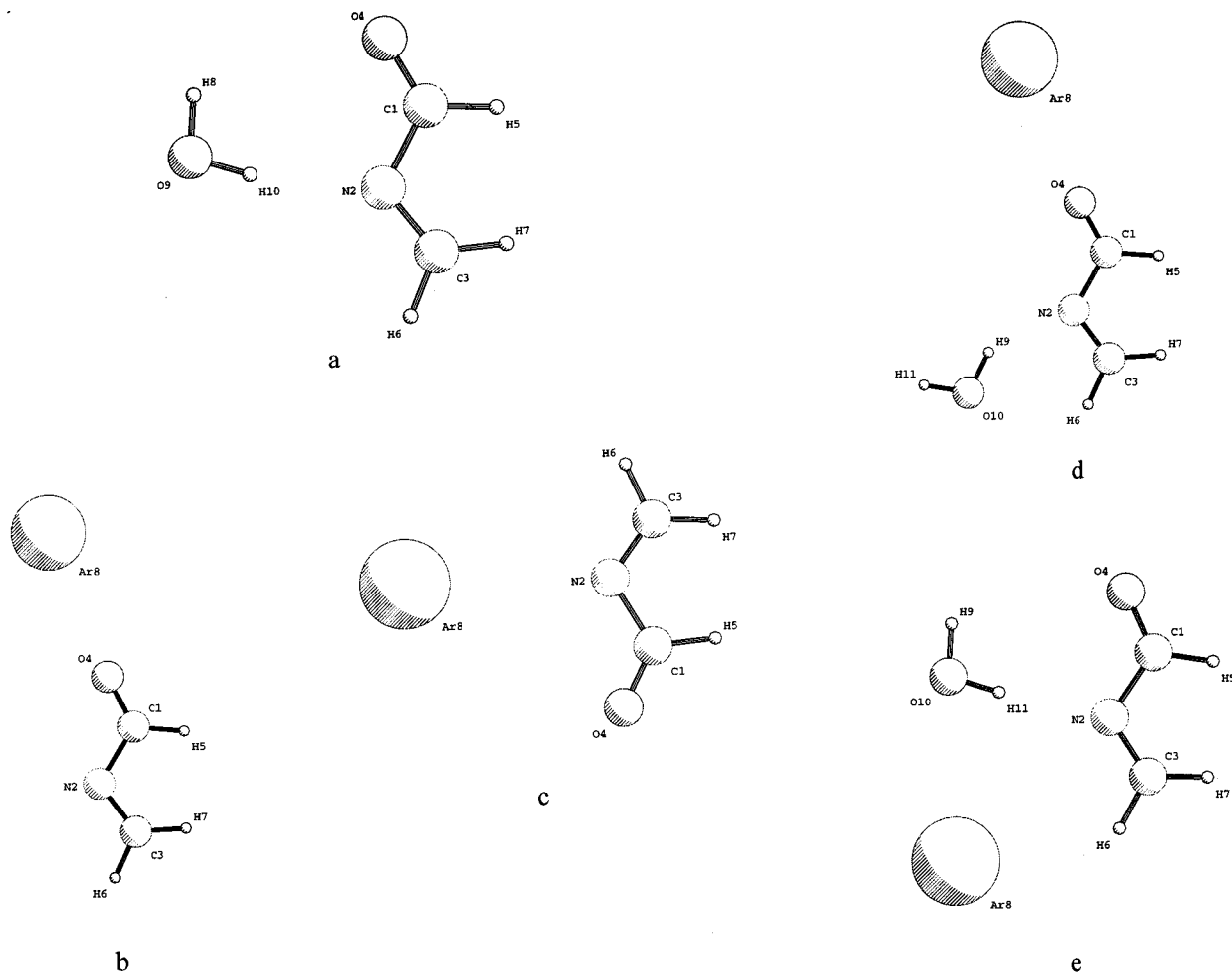
On the basis of the magnitude of the interaction energy in the water·Ar dimer, one can expect that the secondary weaker H bond in the doubly H-bonded structures of water molecule

with MOP may compete with the interaction of an argon atom with water as well as with the argon...MOP interaction. The following calculations have been made to verify this hypothesis.

First, we performed structure optimizations at the MP2/6-31++G** level of theory of the methylformamide complexes with a single water molecule and complexes with a single argon atom. On the basis of the results for the water·argon complex, we can expect that the MP2/6-31++G** level of theory should provide qualitatively correct description of these complexes. We have particularly focused on complexes where the intermolecular interaction involves the proton-accepting centers in methylformamide (N₂ and O₄). The structures of MF·water and MF·Ar complexes, which were obtained from the optimizations, are shown in Scheme 2a,c. As the figures demonstrate, there are two equilibrium MF·Ar structures with the Ar atom interacting with the N₂ and O₄ centers, respectively, and only a single MF·water complex with the water molecule showing a stronger and shorter H bond toward the N₂ center and a weaker H bond with the O₄ center. In the MF·water complex, the HO-H...N and HO-H...O distances are 2.09 and 3.10 Å, respectively. The comparison of these two distances with corresponding distances of the MOP·water complex, which are equal to 2.18 and 2.43 Å, indicates that the secondary H bond is considerably weaker in MF·H₂O than it is in MOP·H₂O.

In the second step we performed geometry optimizations at the MP2/6-31++G** level of theory for two trimers involving MF, water, and argon. The optimization for the first complex was initiated with the argon atom located at O₂ (at the optimal position as determined for the MF·Ar complex) and the water molecule interacting through a single H bond with the N₂ MF center. In the initial structure for the optimization of the second complex, the argon atom was located near the N₂ center (again at its optimal position as determined for the MF·Ar complex) and the water molecule was H bonded to the O₄ center. The

SCHEME 2



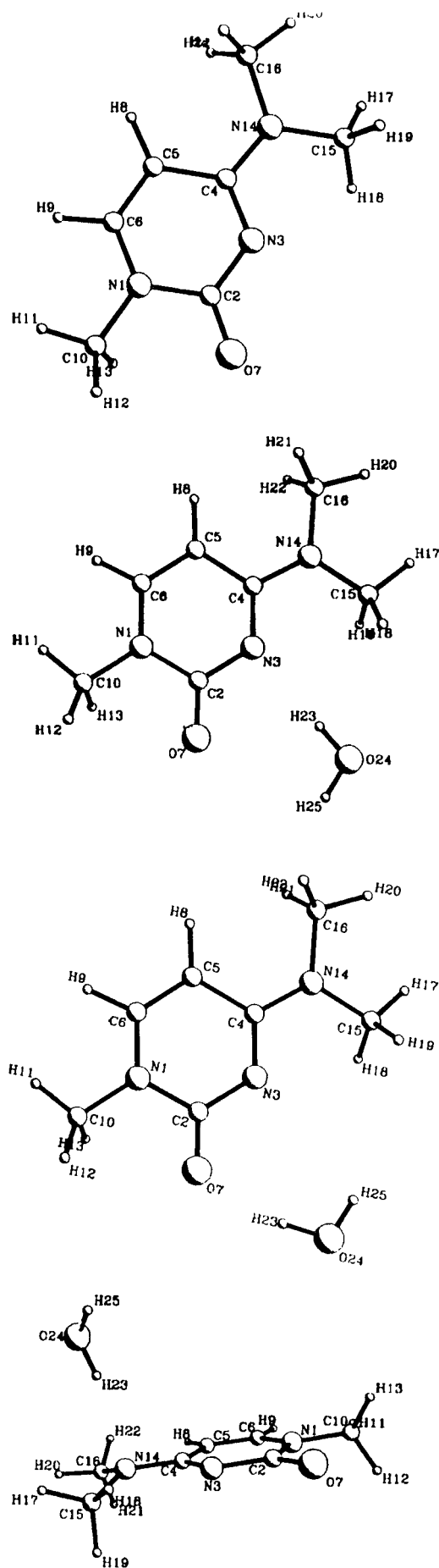
resulting optimal structures of the $\text{MF}\cdot\text{H}_2\text{O}\cdot\text{Ar}$ trimers are shown in Scheme 2d,e. As is seen from the figures, the presence of the argon atom leads to noticeable changes in the $\text{MF}\cdot\text{water}$ interactions, particularly when the argon atom is involved in a complex at the O_4 center. In this case, the secondary H bond disappears, the $\text{HO}-\text{H}\cdots\text{O}$ distance increases to 5.14 Å, and the $\text{N}\cdots\text{H}-\text{OH}$ distance decreases to 2.06 Å. In this complex the $\text{O}\cdots\text{Ar}$ distance is 3.35 Å. The geometry optimization of the second complex with the argon atom placed initially in the vicinity of the nitrogen atom led to a structure which resembles the $\text{MF}\cdots\text{water}$ complex with argon interacting with both the water oxygen and N_2 . In this complex the $\text{HO}-\text{H}\cdots\text{O}$ distance also increases, although much less pronouncedly, to 3.24 Å and the $\text{N}\cdots\text{H}-\text{OH}$ and $\text{N}\cdots\text{Ar}$ distances are 2.08 and 3.84 Å, respectively. In both cases the calculations show that the presence of an argon atom amplifies the $\text{N}\cdots\text{H}-\text{OH}$ interaction and weakens the $\text{O}\cdots\text{H}-\text{OH}$ interaction.

In the next step we calculated the MP2/6-31++G** harmonic IR frequencies for the $\text{MF}\cdot\text{H}_2\text{O}$ dimer and the two $\text{MF}\cdot\text{H}_2\text{O}\cdot\text{Ar}$ trimers. Upon examining the results, we notice a decrease of the frequency of the $\nu_{\text{OH}}^{\text{b}}$ mode and a frequency increase for the $\nu_{\text{OH}}^{\text{f}}$ mode when argon is introduced. The frequencies for the $\nu_{\text{OH}}^{\text{b}}$ mode are 3787, 3778, and 3751 cm^{-1} for the $\text{MF}\cdot\text{water}$ complex without argon, the first and the second $\text{MF}\cdot\text{water}$ trimers involving argon, respectively. The frequency decrease follows the decreasing trend of the $\text{N}\cdots\text{H}-\text{OH}$ distance, reflecting the increasing strength of the $\text{N}\cdots\text{H}-\text{OH}$ H bond. It is apparent, particularly in the first of the two $\text{MF}\cdot\text{H}_2\text{O}\cdot\text{Ar}$ complexes, that the interaction with the argon atom replaces the weaker hydrogen bond and it is also quite possible

that in the $\text{MOP}\cdot\text{water}$ complexes the argon $\cdots\text{O}$ or argon $\cdots\text{N}$ interaction replaces the secondary weaker hydrogen bond. As the result of this competition, the water molecule may form only a single H bond to MOP leading to appearance of spectral features corresponding to the non-H-bonded hydroxy group of water. The increase in the predicted $\nu_{\text{OH}}^{\text{f}}$ frequencies, from 3953 cm^{-1} in the $\text{MF}\cdot\text{water}$ complex to 3955 cm^{-1} in the $\text{MF}\cdot\text{water}\cdot\text{Ar}$ complex, where the argon atom is located near the nitrogen atom, and to 3966 cm^{-1} in the $\text{MF}\cdot\text{water}\cdot\text{Ar}$ complex with the argon atom at O_4 , lends further support to this determination.

TMC/ $\text{H}_2\text{O}/\text{Ar}$. Three types of H-bonded water complexes have been found to be local minima on the potential energy surface at the RHF/6-31++G** level, and these are shown in Scheme 3. Table 7 lists *ab initio* predicted energies and H-bond interaction energies for these three structures. The results indicate that the H-bond interaction at the N_3 atom of TMC leads to the most stable structure with the energy differences relative to the $\text{C}_2=\text{O}\cdots\text{HO}-\text{H}$ and $(\text{CH}_3)_2\text{N}\cdots\text{HO}-\text{H}$ structures being 3.5 and 14 kJ/mol, respectively. The interaction energies calculated for the weak $(\text{CH}_3)_2\text{N}\cdots\text{HO}-\text{H}$ complex (H-bond formed by a hydrogen atom of water and the free electron pair on nitrogen) appear to depend strongly on the method employed. The largest difference is observed between the values obtained at the RHF and the MP2 levels of theory, respectively. At the RHF/BSSE + ZPE level, the interaction energy is only 2 kJ/mol. We attribute the difference between the RHF and MP2 results to the lack of the dispersion interaction effects at the RHF level, which can be significant for this type of complex. In the earlier study of the interactions between water and 4-aminopyridine and 4-aminopyrimidine, the $\text{H}_2\text{N}\cdots\text{HO}-\text{H}$

SCHEME 3



bonding was also found to be about $10 \text{ kJ}\cdot\text{mol}^{-1}$ less stable than the $\text{N}_1\cdots\text{HO}-\text{H}$ and $\text{HN}-\text{H}\cdots\text{OH}_2$ bondings.³

The PA values of the N_3 and O_7 bonding sites in TMC are not known from experiment. However, as for MOP, the PA value of the O_7 site can be estimated rather accurately using the $\Delta\nu_{\text{OH}}/\Delta\text{PA}$ correlation obtained for the H-bonded complexes of phenol with different $\text{C}=\text{O}$ basis in inert solution.³⁰ H-bonding of TMC with phenol occurs also at the $\text{C}_2=\text{O}$ site and is characterized by the thermodynamic parameters, $K = 31 \text{ dm}^3\cdot\text{mol}^{-1}$, $\Delta H = -31 \text{ kJ}\cdot\text{mol}^{-1}$, and $\Delta\nu_{\text{OH}} = -405 \text{ cm}^{-1}$.³¹ These values are all larger than the corresponding values for the MOP-phenol complex, which demonstrates that the carbonyl group of TMC is a stronger proton acceptor than in MOP. Introduction of the frequency shift into the correlation yields an estimated PA value of $953 \text{ kJ}\cdot\text{mol}^{-1}$ for the O_7 site of TMC, which is noticeably larger than the PA value of this site in MOP. The crudely estimated PA value of 959 kJ/mol for the TMC N_3 ³³ site is also much larger than for MOP.

Inspection of the RHF-optimized geometries (Scheme 3) indicates that the H-bonded structures at N_3 and at $\text{C}_2=\text{O}$ are quite different from the corresponding complex structures of MOP. The primary H bond is considerably shorter and stronger for the TMC complexes, while the secondary H bond virtually does not exist. The $\text{N}\cdots\text{H}$ distances are 3.01 \AA for TMC versus 2.56 \AA for MOP in the complex with the primary $\text{OH}\cdots\text{O}=\text{C}$ H bond, and 3.10 \AA for TMC versus 2.69 \AA for MOP in the complex with the primary $\text{OH}\cdots\text{N}_3$ H bond. Furthermore, the computed r_{OH} distances for the OH group of water involved in the primary H bonds are noticeably longer in TMC ($0.949\text{--}0.950 \text{ \AA}$) than in the MOP complexes, while the distance of the other water OH bond, $r_{\text{OH}'}$, is the same as in free water. One can therefore safely state that TMC forms only open $\text{N}\cdots\text{HO}-\text{H}$ and $\text{C}=\text{O}\cdots\text{HO}-\text{H}$ complex structures. This conclusion can be further verified by the analysis of the $\nu_{\text{OH}}^{\text{b}}$ region in the experimental matrix spectra TMC/H O_2/Ar (Figures 7 and 8) in relation to the corresponding spectral results described for MOP/H $_2\text{O}/\text{Ar}$. At very low water content only a few water-induced absorptions are observed in the high frequency region: 3705 and 3701 cm^{-1} (water $\nu_{\text{OH}}^{\text{f}}$, Figure 8b) and $3465/3440 \text{ cm}^{-1}$ (water $\nu_{\text{OH}}^{\text{b}}$, Figure 7b). The most important complex bands observed in the fingerprint region of that spectrum are located at 1620 and 1616 cm^{-1} (water bending mode), 1693 and 1676 cm^{-1} ($\nu_{\text{C}=\text{O}}(-5/-22 \text{ cm}^{-1})$), and 787 cm^{-1} ($\gamma_{\text{C}=\text{O}}(+6 \text{ cm}^{-1})$). It should be mentioned that the $\nu_{\text{C}=\text{O}}$ complex band at 1693 cm^{-1} overlaps with the Fermi component of the free $\nu_{\text{C}=\text{O}}$ mode, which is manifested by intensity increase and some broadening. All these new absorptions indicate that at least two different H-bond complexes are present in the Ar matrix. That the $\text{C}_2=\text{O}$ site takes part in the H-bond interaction is obvious from a frequency decrease of the $\nu_{\text{C}=\text{O}}$ mode and a frequency increase of the $\gamma_{\text{C}=\text{O}}$ mode. In view of the spectral assignment for MOP-H $_2\text{O}$ in terms of two open $\text{C}_2=\text{O}\cdots\text{HO}-\text{H}$ and $\text{N}_3\cdots\text{HO}-\text{H}$ complexes discussed in the previous section (with the $\nu_{\text{OH}}^{\text{b}}$ shift of about 40 cm^{-1} and the $\nu_{\text{OH}}^{\text{f}}$ shift of 4 cm^{-1}), we now assign the doublet observed in the region $3470\text{--}3440 \text{ cm}^{-1}$ and two bands found in the water ν_3 region to the $\nu_{\text{OH}}^{\text{b}}$ and $\nu_{\text{OH}}^{\text{f}}$ modes of similar two open complexes of TMC. As for MOP and other systems examined earlier,³³ the most displaced water bands, *i.e.*, the trio of bands 3701 , 3440 , 1620 cm^{-1} , were assigned to the complex at the N_3 site. This is also consistent with the position of the $\nu_{\text{OH}}^{\text{b}}$ band for the $\text{C}_2=\text{O}\cdots\text{HO}-\text{H}$ complex of TMC observed in 1,2-dichloroethane (see further). A smaller $\nu_{\text{OH}}^{\text{b}}$ frequency for TMC as compared to MOP is consistent with the noticeably larger PA value of the TMC $\text{C}=\text{O}$ site compared to MOP. The order of magnitude

TABLE 7: *N,N*,1-Trimethylcytosine (TMC) and Its Complexes with Water. Total (au) and Relative (kJ·mol⁻¹) Energies Calculated with the 6-31++G Basis Set^a**

	TMC	N ₃ ···HO-H	C=O···HO-H	H ₂ N···HO-H
SCF	-509.7281684	-585.7722519	-585.7713167	-585.7642381
MP2 ^b	-511.3638655	-587.6128813	-587.6112642	-587.6070278
SCF (base with ghost water orbitals)		-509.7284552	-509.7284875	-509.7286262
MP2 (base with ghost water orbitals)		-511.3649635	-511.3648765	-511.3654245
SCF (water with ghost base orbitals)		-76.0324569	-76.0322758	-76.0326212
MP2 (water with ghost base orbitals)		-76.2354345	-76.2349036	-76.2360514
ZPE ^c	0.1760192	0.1997509	0.1994566	0.1991361
total	-511.1878463	-587.4131304	-587.4118076	-587.4078917
ΔE^d		0.0	3.47	13.75
H-bond energy (SCF/BSSE+ZPE)		-22.08	-20.78	-1.77
H-bond energy (MP2/BSSE+ZPE)		-25.08	-23.23	-8.49
μ (D)	6.85	8.39	10.08	5.47

^a All molecular geometries optimized at the SCF/6-31++G** level (Scheme 2). ^{b-d} See Table 3, footnotes b, c, d.

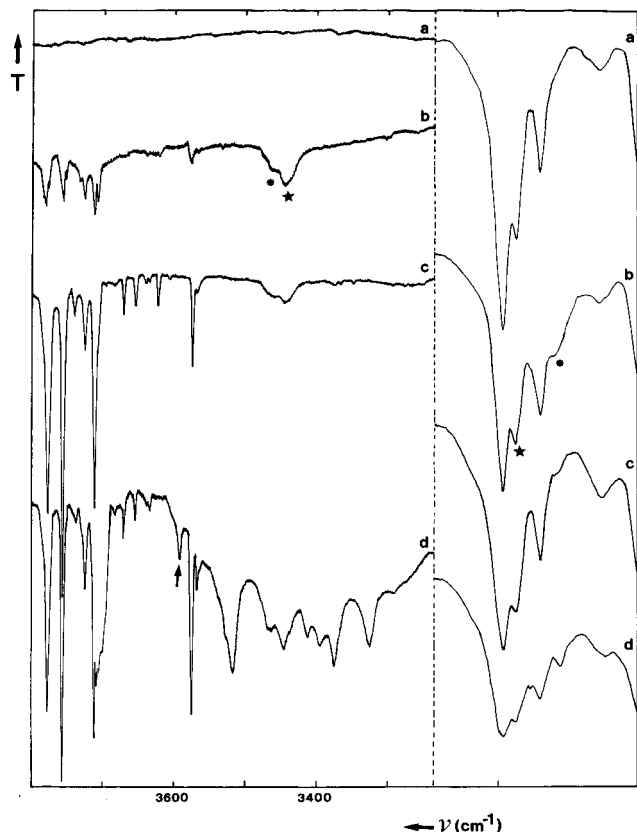


Figure 7. ν_3 - ν_1 (H₂O) and ν^b_{OH} region (left) and the $\nu_{C=O}$ region (right) of the FT-IR spectrum of *N,N*,1-trimethylcytosine/H₂O/Ar at 12 K (a, monomer base; b, H₂O/Ar = impurity level; c, H₂O/Ar = 1/500; d, H₂O/Ar = 1/100 annealed; *, C₂=O···HO-H complex; ★, N₃···HO-H complex; †, (CH₃)₂N···HO-H complex; D, T, P: water dimer, trimer, polymer).

of the $\Delta\nu_{C=O}$ and $\Delta\gamma_{C=O}$ frequency shifts are similar to that found in the uracil C=O···HO-H complex in Ar.³⁴ The δ -(HOH) and ν^f_{OH} modes for the C₂=O···H-OH TMC complex are assigned to the bands found at 1616 and 3705 cm⁻¹, respectively. On the other hand, from the large PA(N₃) value for TMC, one should expect the corresponding frequency for the N₃···HO-H complex to be even further decreased than 3440 cm⁻¹. Table 5 indicates, however, that the N···H distance for the N₃···HO-H complex is markedly longer than the O···H distance for the C₂=O···HO-H complex, and even longer than in pyrimidine·H₂O which has the ν^b_{OH} frequency of 3468 cm⁻¹ (!). The ν^b_{OH} frequency for the N₃···HO-H complex of TMC is also higher than the values found for the N₃···HO-H complexes of 1-methylcytosine⁷ and cytosine,⁸ which seems to be in conflict with the notion of electron-donating effect of the CH₃ groups on N₁₄. This effect is expected to increase the N₃

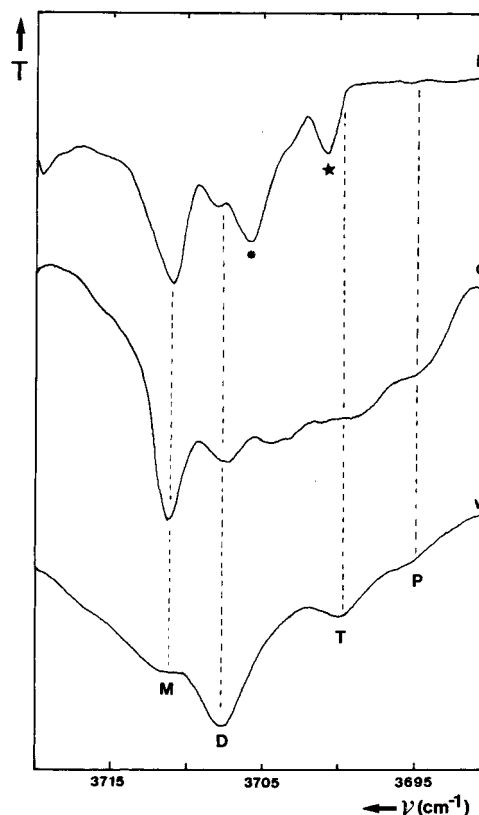


Figure 8. ν_3 (H₂O) region of the FT-IR spectrum of *N,N*,1-trimethylcytosine/H₂O/Ar (b, d, cf. Figure 7) compared to H₂O/Ar (w: 1/200) at 12 K (M, D, T, P: water monomer, dimer, trimer, polymer; *, C₂=O···HO-H complex; ★, N₃···HO-H complex).

basicity in TMC. However, this kind of reasoning is not strictly valid since, as we will demonstrate for 1-methylcytosine and cytosine, closed N₃···H-O···H-NH complexes are formed there and the H-bond cooperativity effect in these systems results in shorter H-bond distances and larger frequency shifts for the bridged OH bond.^{7,8} Steric hindrance of the CH₃ groups at N₁₄ may also influence the accessibility of the N₃ lone pair, which in turn can also contribute to a longer H-bond distance. Other spectral manifestations for the N₃···HO-H complex are the δ -(HOH) and ν^f_{OH} bands at 1620 and 3701 cm⁻¹. However, no supporting argument for this complex can be obtained from the shifted ν (N₃=C₄) mode because of a large number of bands present in the 1550–1500 cm⁻¹ spectral region.

We have also investigated the H-bond interaction of H₂O with TMC in 1,2-dichloroethane solution at ambient temperature. The corresponding FT-IR spectrum is shown in Figure 9. One observes a strong complex absorption at 3423 cm⁻¹, with a low-frequency shoulder at about 3300 cm⁻¹. The main complex

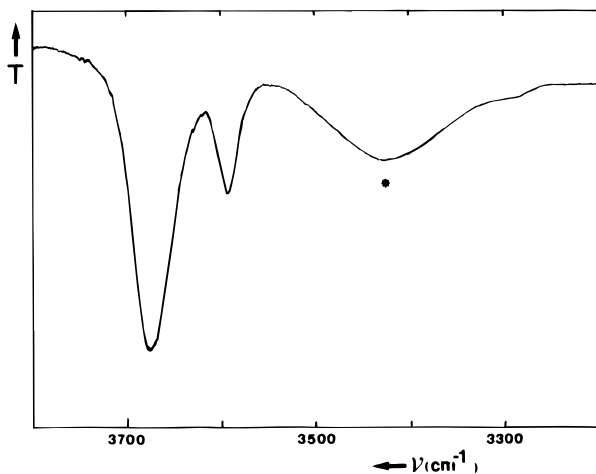


Figure 9. Water stretching region of the FT-IR spectrum of a ternary solution *N,N*,1-trimethylcytosine/H₂O/1,2-dichloroethane at room temperature ($C_{\text{base}} = 0.046 \text{ mol}\cdot\text{dm}^{-3}$; $C_{\text{water}} = 0.050 \text{ mol}\cdot\text{dm}^{-3}$).

absorption is due to the $\nu_{\text{OH}}^{\text{b}}$ mode in the $\text{C}_2=\text{O}\cdots\text{HO}-\text{H}$ complex, since the corrected shift (-195 cm^{-1}) is again somewhat smaller than that in Ar (-202 cm^{-1}). Our earlier and tentative interpretation of the shoulder as resulting from the alternative complex $\text{N}_3\cdots\text{HO}-\text{H}^{33}$ can now be rejected based on the *ab initio* results, since the shift for such a complex should be much larger in solution (-321 cm^{-1}) than in Ar (-231 cm^{-1}). We therefore prefer to reassign the shoulder to higher stoichiometry H-bonded complexes in solution, which are probably formed at higher water concentration.

Table 8 summarizes the *ab initio* (RHF) calculated spectral data for the three TMC complexes shown in Scheme 3. Calculated shifts with respect to the monomer TMC frequencies are similar for the $\text{N}_3\cdots\text{H}-\text{OH}$ and $\text{C}_2=\text{O}\cdots\text{H}-\text{OH}$ complexes. Contrary to MOP, where a comparison between calculated shifts ("closed" complexes) and experimental shifts (open complexes observed in the matrix spectra) could not be made, the theoretical and experimental data can be compared for the water complexes of TMC. This is illustrated by the predicted asymmetrical shift $\Delta\nu_{\text{C}=\text{O}} = -5/-21$, which is nicely reproduced in the experimental matrix spectrum ($-5/-22$) (Figure 7). However, it is also clear that this comparison cannot be extended at the quantitative level for all the modes of the bonded H₂O molecule, since a small degree of the secondary H bonding is still present in the TMC complexes, as predicted theoretically. This is clearly illustrated in Figure 10 which shows the correlation between the scaling factor of the theoretically-predicted $\nu_{\text{OH}}^{\text{b}}$ mode and the experimental (Ar matrix), corrected frequency shifts of this mode in different $\text{N}\cdots\text{HO}-\text{H}$ complexes of a series of N-basis and in $(\text{H}_2\text{O})_2$.²⁷ The point corresponding to the $\text{N}_3\cdots\text{HO}-\text{H}$ complex of TMC ($0.843/231 \text{ cm}^{-1}$) in Figure 10 slightly deviates from the correlation for open complexes. This indicates that the predicted frequency for the weakly $\text{C}_2=\text{O}$ bonded complex is higher than the frequency that should be found in the open complex. However, the much larger deviation for the MOP $\text{N}_3\cdots\text{HOH}$ complex ($0.836/216 \text{ cm}^{-1}$ in Figure 10) demonstrates that the difference between the structure of the predicted $\text{N}_3\cdots\text{H}-\text{O}-\text{H}\cdots\text{O}=\text{C}_2$ complex and the experimentally observed open complex is noticeably larger(!). We believe that such deviations clearly reflect the anti-cooperativity in "this nearly closed" H-bonded system.

When the amount of water in the Ar matrix increases, an additional absorption band appears at 3590 cm^{-1} (Figure 7d). This band can be assigned either to the $\nu_{\text{OH}}^{\text{b}}$ mode of the $(\text{CH}_3)_2\text{N}\cdots\text{H}-\text{OH}$ complex with the predicted $\nu_{\text{OH}}^{\text{b}}$ frequency of 4118 cm^{-1} ($\nu^{\text{exp}}/\nu^{\text{theor}}$ scaling factor 0.872) or, similar to what

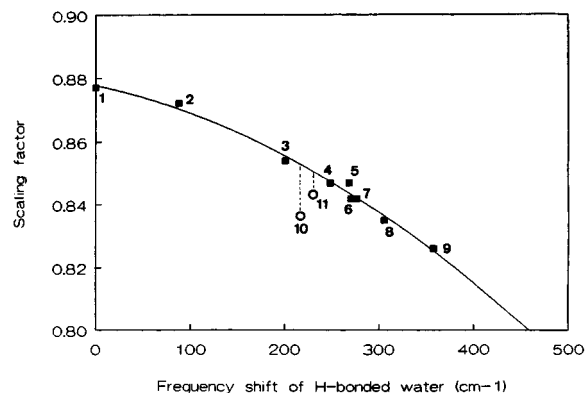


Figure 10. Correlation between the optimal scaling factor $\nu^{\text{exp}}/\nu^{\text{theor}}$ and the corrected frequency shift of the bonded water mode $\nu_{\text{OH}}^{\text{b}}$ in H-bonded complexes $\text{B}\cdots\text{HO}-\text{H}$ (■, taken from ref 12; 1 = free water; 2 = water dimer; 3 = pyrimidine·H₂O; 4 = 4-aminopyrimidine·H₂O; 5 = 3-hydroxypyridine·H₂O; 6 = pyridine·H₂O; 7 = imidazole·H₂O; 8 = 4-hydroxypyridine·H₂O; 9 = 4-aminopyridine·H₂O; ○ = complexes $\text{N}_3\cdots\text{HO}-\text{H}$ studied in this work; 10 = 1-methyl-2-pyrimidine·H₂O; 11 = *N,N*,1-trimethylcytosine·H₂O).

was proposed for MOP, to the "slightly closed" complex with the predicted $\nu_{\text{OH}}^{\text{b}}$ frequencies of $4079/4069 \text{ cm}^{-1}$ (scaling factor 0.881). We prefer the first alternative, since the scaling factor for the closed MOP complexes ($4127/4123$ compared to the experimental frequency 3589 cm^{-1}) is 0.870, which is similar to the value expected for the H₂O molecule with slightly different OH bonds are involved in a weak intermolecular complex. Since the strength of the secondary H bonding is much smaller in the TMC complexes, the scaling factor should fall between 0.870 (MOP) and 0.847 (open TMC complexes), being probably relatively closer to the latter value. This is, however, contradictory to the value of 0.881 calculated above. Furthermore, the latter value is larger than that for free water (Table 5), which must be rejected on physical grounds.

1:2 Complexes in Water-Rich Ar Matrices. We again return to the question, why in the experiment at low temperature the *ab initio*-predicted most stable complexes of MOP are not formed, but instead open, less stable complexes are present? It is well-known that formation of a low-temperature matrix by rapid condensation of the vapor phase from ambient to cryogenic temperatures normally does not yield the most stable matrix crystal structure.³⁷ Annealing of the matrix usually results in formation of more stable crystal structures, but this process also causes less stable intermolecular complexes to convert to more stable ones, *e.g.*, the amount of the less stable $\text{C}(=\text{O})-\text{O}\cdots\text{HCl}$ complex of methyl acetate decreases in favor of the more stable structure $\text{C}(\text{O})=\text{O}\cdots\text{HCl}$.^{35,38} It is therefore not surprising that open complexes are observed instead of the more stable, "closed" ones, at least initially. It was our intention to apply the technique of matrix annealing in this work in order to possibly convert the open complexes into the "closed" ones. However, upon annealing of the matrix, a relatively large amount of dimers, trimers, *etc.*, of water are also formed by diffusion, and this increases the probability of formation of higher-stoichiometry complexes $\text{B}(\text{H}_2\text{O})_n$. In the case of MOP, additional bands appear after annealing of the water-rich sample at 3410 and 3390 cm^{-1} , while in the same time the band at 3590 cm^{-1} assigned to the closed complex almost disappears (Figure 3). This is consistent with the hypothesis of formation of 1:2 complexes $\text{C}_2=\text{O}\cdots\text{H}-\text{O}\cdots\text{HOH}$ (3410), $\text{N}_3\cdots\text{H}-\text{O}\cdots\text{HO}-\text{H}$ (3390), as well as closed $\text{N}_3\cdots\text{H}-\text{O}(\cdots\text{HO}-\text{H})-\text{O}=\text{C}$ (or vice versa) structures (intensity decrease of the 3590 cm^{-1} band). Comparison of the shifts for the bridged H-O stretching bands in the 1:2 complexes with the shifts of the corresponding

TABLE 8: Calculated (SCF/6-31++G) Spectral Data for the N₃···HO—H and C₂=O···HO—H Bonded Complexes of N,N,N,1-Trimethylcytosine with Water**

N ₃ ⋯HO—H		C ₂ =O⋯HO—H		N ₁₄ ⋯HO—H		PED ^b
<i>ν</i> (cm ^{−1}) ^a	<i>I</i> (km/mol)	<i>ν</i> (cm ^{−1}) ^a	<i>I</i> (km/mol)	<i>ν</i> (cm ^{−1}) ^a	<i>I</i> (km/mol)	
Water Modes						
4224	146	4231	59	4242	182	<i>ν</i> ^l (OH) (76) + <i>ν</i> ^b (OH) (22)
4079	311	4069	300	4118	120	<i>ν</i> ^b (OH) (78) + <i>ν</i> ^l (OH) (23)
1776	106	1790	177	1748	75	δ(HOH) (90)
601	149	625	162	436	100	o.o.p. wag HOH (92)
289	102	261	70	248	48	δ(O⋯HO) (81)
236	61	147	27	216	46	τ(HOH) (74) + o.o.p. wag HOH (12)
113	8	131	23	148	125	<i>ν</i> (O⋯HO) (92)
56	9	24	2	29	5	i.p. butterfly (101)
14	0.5	17	2	15	10	o.o.p. butterfly (83)
Base Modes						
3098 (+1)	1	3097 (0)	1	3103 (+6)	1	<i>ν</i> (C ₅ H) (97)
3046 (+3)	6	3047 (+4)	5	3046 (+3)	6	<i>ν</i> (C ₆ H) (96)
2980	48	2994	15	3019	3	<i>ν</i> ^d ₁ (CH ₃) at C ₁₅ (96)
2978	15	2980	14	2978	15	<i>ν</i> ^d ₂ (CH ₃) at C ₁₀ (96)
2976	17	2980	27	2976	27	<i>ν</i> ^d ₁ (CH ₃) at C ₁₆ (100)
2973	5	2977	16	2976	14	<i>ν</i> ^d ₁ (CH ₃) at C ₁₀ (88)
2966	17	2947	32	2943	47	<i>ν</i> ^d ₂ (CH ₃) at C ₁₅ (79) + <i>ν</i> ^s (CH ₃) at C ₁₅ (12)
2915	39	2918	37	2938	16	<i>ν</i> ^d ₂ (CH ₃) at C ₁₆ (98)
2900	42	2901	49	2900	50	<i>ν</i> ^s (CH ₃) at C ₁₀ (93)
2899	41	2875	49	2861	83	<i>ν</i> ^s (CH ₃) at C ₁₅ (88) + <i>ν</i> _s (CH ₃) at C ₁₅ (12)
2866	63	2865	64	2855	46	<i>ν</i> ^s (CH ₃) at C ₁₆ (99)
1716 (−5)	931	1700 (−21)	1018	1724 (+3)	1007	<i>ν</i> (CO) (70)
1646 (−2)	668	1646 (−2)	602	1649 (+1)	667	<i>ν</i> (C ₅ C ₆) (38) + <i>ν</i> (N ₃ C ₄) (12) + δ(C ₆ H) (13)
1525 (+4)	353	1523 (+2)	322	1522 (+1)	321	<i>ν</i> (C ₄ C ₅) (18) + <i>ν</i> (C ₄ N) (14) + δ(C ₅ H) (12) + <i>ν</i> (C ₆ N ₁) (12)
1517 (+2)	392	1515 (0)	494	1508 (−7)	265	<i>ν</i> (N ₃ C ₄) (21) + <i>ν</i> (C ₄ N) (12)
1484	18	1484	17	1482	19	δ ^d ₁ (CH ₃) + C ₁₆ (65)
1474	3	1472	2	1473	8	δ ^d ₁ (CH ₃) at C ₁₀ (30) + δ ^d ₂ (CH ₃) at C ₁₅ (31) + δ ^d ₁ (CH ₃) + C ₁₅ (14)
1468	15	1471	13	1469	7	δ ^d ₁ (CH ₃) at C ₁₀ (36) + δ ^d ₂ (CH ₃) at C ₁₅ (12)
1464	11	1463	15	1464	13	δ ^d ₂ (CH ₃) at C ₁₆ (85)
1450	7	1450	6	1456	10	δ ^d ₁ (CH ₃) at C ₁₅ (56) + δ ^d ₂ (CH ₃) at C ₁₅ (21)
1450	68	1449	53	1448	25	δ ^s (CH ₃) at C ₁₆ (37) + δ ^s (CH ₃) at C ₁₀ (25)
1440	7	1444	7	1439	7	δ ^d ₂ (CH ₃) at C ₁₀ (92)
1427	95	1427	89	1427	36	δ ^s (CH ₃) at C ₁₀ (53) + δ ^s (CH ₃) at C ₁₆ (28)
1422	40	1419	54	1416	29	δ ^s (CH ₃) at C ₁₅ (71) + δ ^s (CH ₃) at C ₁₆ (16)
1380 (−4)	412	1380 (−4)	399	1369 (−11)	413	<i>ν</i> (C ₄ N) (22)
1339 (+2)	94	1339 (+2)	99	1334 (0)	105	δ(C ₆ H) (26) + <i>ν</i> (C ₂ N ₃) (13)
1291 (+4)	9	1290 (+3)	8	1283 (−4)	17	<i>ν</i> ^a (C ₁₅ N ₁₄ C ₁₆) (15) + <i>ν</i> (C ₂ N ₃) (11) + <i>ν</i> (N ₃ C ₄) (15)
1242 (+12)	83	1241 (+11)	80	1223 (−7)	43	<i>ν</i> ^a (C ₁₅ N ₁₄ C ₁₆) (23) + <i>ν</i> (N ₁ C ₂) (16) + <i>ν</i> (C ₂ N ₃) (14)
1200 (0)	18	1200 (0)	18	1198 (−2)	29	δ(C ₅ H) (31) + <i>ν</i> (N ₁ C ₁₀) (23) + δ _{R1} (12)
1180 (0)	1	1181 (+1)	0.02	1179 (−1)	5	δ(C ₆ H) (19) + ρ ₁ (CH ₃) at C ₁₆ (20)
1129	65	1131	10	1141	31	ρ ₂ (CH ₃) at C ₁₅ (35) + ρ ₂ (CH ₃) at C ₁₆ (16)
1127	2	1127	2	1128	2	ρ ₂ (CH ₃) at C ₁₀ (90)
1119	3	1120	94	1112	147	ρ ₂ (CH ₃) at C ₁₆ (22) + ρ ₁ (CH ₃) at C ₁₅ (27)
1110	0.1	1108	3	1098	21	ρ ₂ (CH ₃) at C ₁₆ (55) + ρ ₂ (CH ₃) at C ₁₅ (21) + ρ ₁ (CH ₃) at C ₁₅ (16)
1052	29	1053	33	1050	29	ρ ₁ (CH ₃) at C ₁₆ (30) + <i>ν</i> ^a (C ₁₅ N ₁₄ C ₁₆) (29) + ρ ₁ (CH ₃) at C ₁₅ (15) + ρ ₂ (CH ₃) at C ₁₅ (14)
1042	8	1042	5	1041	4	ρ ₁ (CH ₃) at C ₁₀ (33) + <i>ν</i> (C ₆ N ₁) (16) + δ _{R1} (12)
1000 (+3)	0.8	997 (0)	1	999 (+2)	1	γ(C ₆ H) (97) + γ(C ₅ H) (16)
986 (+7)	23	987 (+8)	16	978 (−1)	15	<i>ν</i> (C ₄ C ₅) (32) + <i>ν</i> (N ₁ C ₂) (19)
904 (−3)	5	907 (0)	7	903 (−4)	15	<i>ν</i> ^s (C ₁₅ N ₁₄ C ₁₆) (48) + δ _{R1} (23)
791 (+2)	64	794 (+5)	70	794 (+5)	68	γ(C=O) (82) + τ _{R1} (16)
774 (+4)	47	775 (+5)	40	776 (+6)	33	γ(C ₄ N) (47) + γ(C ₅ H) (46)
753 (−1)	3	757	3	756 (+2)	4	<i>ν</i> (N ₁ C ₁₀) (26) + <i>ν</i> (N ₁ C ₂) (20)
706 (+2)	12	707	13	706 (+2)	15	γ(C ₅ H) (39) + γ(C ₄ N) (26) + τ _{R1} (18)
696 (+4)	8	697	7	692 (0)	3	<i>ν</i> ^s (C ₁₅ N ₁₄ C ₁₆) (23) + δ _{R1} (14)
602 (+1)	9	604	11	602 (+1)	6	δ _{R3} (23) + δ(C=O) (21) + δ(N ₁ C ₁₀) (15) + (δC ₄ N) (14)
576 (+6)	7	574	14	569 (−1)	2	δ _{R3} (46)
510 (+13)	3	508	4	501 (+4)	9	δ(C ₁₅ N ₁₄ C ₁₆) (39) + δ _{R2} (26)
425	7	430	14	429 (+2)	7	ρ(C ₁₅ N ₁₄ C ₁₆) (29) + δ(C=O) (15) + δ _{R2} (13)
425 (+2)	9	426	4	425 (+2)	13	τ _{R2} (47) + τ _{R1} (23)
350 (−2)	2	353	1	361 (+9)	2	δ _{R2} (27) + δ(C ₁₅ N ₁₄ C ₁₆) (37) + <i>ν</i> (C ₄ N) (13)
330	8	340	13	331	8	δ(N ₁ C ₁₀) (60) + δ(C=O) (11)
275	7	271	3	280	9	γ(N ₁ C ₁₀) (31) + wag (C ₁₅ N ₁₄ C ₁₆) (13) + τ _{R2} (13) + τ _{R3} (14) + τ(CH ₃) at C ₁₆ (16)
204	5	207	14	230	30	δ(C ₄ N) (30) + ρ(C ₁₅ N ₁₄ C ₁₆) (14) + (17) water
201	15	199	1	165	13	γ(N ₁ C ₁₀) (49) + τ _{R2} (14)
183	13	185	11	147	19	τ _{R1} (23) + τ(C ₁₅ N ₁₄ C ₁₆) (19) + τ(CH ₃) at C ₁₆ (21)
133	2	116	1	116	0.4	τ(CH ₃) at C ₁₀ (64)
106	1	91	3	109	0.4	wag (C ₁₅ N ₁₄ C ₁₆) (27) + τ _{R3} (21) + τ(CH ₃) at C ₁₆ (20) + τ(CH ₃) at C ₁₀ (12)
83	0.7	81	1	90	1	τ _{R3} (33) + τ _{R2} (15) + τ(CH ₃) at C ₁₆ (17) + τ(C ₁₅ N ₁₄ C ₁₆) (20)
70	5	71	13	78	10	wag (C ₁₅ N ₁₄ C ₁₆) (36) + τ(C ₁₅ N ₁₄ C ₁₆) (14) + τ _{R3} (32)
48	0.1	55	4	66	3	τ(CH ₃) at C ₁₅ (53) + τ(C ₁₅ N ₁₄ C ₁₆) (15)

^a See Table 5. ^b PEDs for the C₂=O···HO—H complex. ^c See Table 5.

open 1:1 complexes yields the cooperativity factor¹⁴ of about 1.4 (C=O complex) and about 1.3 (N₃ complex). These are quite acceptable values for linear 1:2 complexes of water, for which the mean cooperativity factor of 1.35 was found.¹⁴ The ν_{OH} mode of the end H₂O molecule in the 1:2 complex is usually found at slightly smaller frequency than the donor mode in the dimer HO-H...OH₂, and this explains the low-frequency split of the dimer donor band (3574 cm⁻¹) at 3567 cm⁻¹ (Figure 3).

In the case of TMC, it is clear (spectrum d in Figures 7 and 8) that the same bands at 3410 and 3390 cm⁻¹ also appear on annealing. Also, the band at 3590 cm⁻¹, which was not present before, now appears(!). This observation supports the assignment of the 3590 cm⁻¹ band to the (CH₃)₂N...HO-H complex instead of to the slightly closed 1:1 complex, since the amount of the latter should decrease on annealing. For the TMC 1:2 C=O...H-O...HO-H and N₃...H-O...HO-H complexes, the cooperativity factor of about 1.25 is found, again not far from the mean value of 1.35 in the linear B...H-O...HO-H complexes.¹⁴

Summary

The combined FT-IR matrix-isolation and theoretical *ab initio* method has been used to investigate the H-bond interaction of the nontautomeric, polyfunctional basis 1-methyl-2-pyrimidone and *N,N*,1-trimethylcytosine with water. The *ab initio* results indicate a significant degree of secondary H-bonding for the N₃...HO-H and the C₂=O...HO-H complexes of the former base. The anticooperativity between the two H bonds in these complexes results in relatively small predicted frequency shifts of the bonded water modes. Contrary to these predictions, open N₃...HO-H and C₂=O...HO-H complexes with larger frequency shifts of the water modes are observed in low-temperature matrix. This feature can be explained by taking into account the water...Ar interaction. Annealing induces formation of linear 1:2 complexes instead of formation of the closed structures. The *ab initio* predicted stable complexes at the N₃ or C₂=O site of *N,N*,1-trimethylcytosine are characterized by a much smaller degree of the secondary H bonding, and a comparison can be made with the experimental spectral data obtained in Ar. The (CH₃)₂N...HO-H complex, which is considerably less stable, was only identified in water-rich matrices.

Acknowledgment. This work was supported by the NATO International Collaborative Grant INT-9313268. J.S. acknowledges the Belgian IWONL for a Ph.D. research grant. L.A. acknowledges support from the Office of Health and Environmental Research, Office of Energy Research, Department of Energy (Grant No. DEFG 0393ER61605). L.A. thanks the Swedish Natural Science Research Council for supporting his stay with the Theoretical Chemistry group at the University of Lund, and Professor B. Roos for his hospitality. G.M. acknowledges the Belgian NFWO for a permanent Research

Fellowship. The authors also acknowledge Dr. L. Lapinski (Polish Academy of Sciences, Warsaw, Poland) for providing the PED program.

References and Notes

- (1) Destexhe, A.; Smets, J.; Adamowicz, L.; Maes, G. *J. Phys. Chem.* **1994**, *98*, 1506.
- (2) Smets, J.; Adamowicz, L.; Maes, G. *J. Mol. Struct.* **1994**, *322*, 113.
- (3) Smets, J.; Adamowicz, L.; Maes, G. *J. Phys. Chem.* **1995**, *99*, 6387.
- (4) Buyl, F.; Smets, J.; Maes, G.; Adamowicz, L. *J. Phys. Chem.* **1995**, *99*, 14967.
- (5) Szczesniak, M.; Kwiatkowski, J. S.; KuBulat, K.; Szczepaniak, K.; Person, W. B. *J. Am. Chem. Soc.* **1988**, *110*, 8319.
- (6) Lapinski, L.; Nowak, M. J.; Fulara, J.; Les, A.; Adamowicz, L. *J. Phys. Chem.* **1990**, *94*, 6555.
- (7) Smets, J.; Adamowicz, L.; Maes, G. *J. Phys. Chem.* **1996**, *100*, 6434.
- (8) Vranken, H.; Smets, J.; Maes, G.; Adamowicz, L., to be published.
- (9) Held, A.; Pratt, D. W. *J. Am. Chem. Soc.* **1993**, *115*, 9715.
- (10) Del Bene, J. E. *J. Phys. Chem.* **1994**, 5902.
- (11) Field, M. J.; Hillier, I. H. *J. Chem. Soc., Perkin Trans. 2* **1967**, 617.
- (12) Smets, J.; Destexhe, A.; Maes, G.; Adamowicz, L. *J. Phys. Chem.*, in press.
- (13) Vranken, H.; Smets, J.; Adamowicz, L.; Maes, G., to be published.
- (14) Maes, G.; Smets, J. *J. Phys. Chem.* **1993**, *97*, 1818.
- (15) Smets, J.; McCarthy, W.; Maes, G.; Adamowicz, L. *THEOCHEM*, submitted for publication.
- (16) Maes, G. *Bull. Soc. Chim. Belg.* **1981**, *90*, 1093.
- (17) Graindourze, M.; Smets, J.; Zeegers-Huyskens, Th.; Maes, G. *J. Mol. Struct.* **1990**, *222*, 345.
- (18) Curd, F. H.; Richardson, D. N. *J. Chem. Soc.* **1955**, 1853.
- (19) Kenner, G. W.; Reese, L. B.; Todd, A. R. *J. Chem. Soc.* **1955**, 855.
- (20) Hilbert, G. E.; Johnson, T. B. *J. Am. Chem. Soc.* **1930**, 2001.
- (21) GAUSSIAN 92; Frisch, C. PM. J.; Trucks, G. W.; Head-Gordon, M.; Gill, P. M. W.; Wong, W. M.; Foresman, J. B.; Johnson, B. G.; Schlegel, H. B.; Robb, M. A.; Replogie, E. S.; Gomperts, R.; Andres, J. L.; Raghavachari, K.; Binkley, J. S.; Gonzales, C.; Martin, R. L.; Fox, D. J.; Defrees, D. J.; Baker, J.; Stewart, J. J. P.; Pople, J. A. Gaussian Inc.: Pittsburgh, PA, 1992.
- (22) Chalasinski, G.; Szczesniak, M. M. *Chem. Rev.* **1994**, *94*, 1723.
- (23) Del Bene, J. E.; Person, W. B.; Szczepaniak, K. *J. Phys. Chem.* **1995**, *99*, 10705.
- (24) Kasende, O.; Zeegers-Huyskens, Th. *J. Phys. Chem.* **1984**, *88*, 2636.
- (25) Maes, G.; Smets, J. *Vibrat. Spectrosc.* **1992**, *3*, 21.
- (26) Wojcik, M. J.; Rostkowska, H.; Szczepaniak, K.; Person, W. B. *Spectrochim. Acta A* **1989**, *45*, 499.
- (27) Van Bael, M. K.; Schoone, K.; L. Houben; Smets, J.; McCarthy, W.; Adamowicz, L.; Nowak, M. J.; Maes, G. *J. Phys. Chem.*, in press.
- (28) Lias, S. G.; Liebman, J. F.; Levin, R. D. *J. Phys. Chem. Ref. Data* **1984**, *13*, 695.
- (29) Huyskens, P. L. *J. Am. Chem. Soc.* **1977**, *99*, 2578.
- (30) Zeegers-Huyskens, Th., personal communication.
- (31) Kasende, O. Ph.D. Thesis, University of Leuven, 1983.
- (32) Kasende, O.; Zeegers-Huyskens, Th. *J. Phys. Chem.* **1984**, *88*, 2636.
- (33) Maes, G.; Smets, J. *J. Mol. Struct.* **1992**, *270*, 141.
- (34) Graindourze, M.; Grootaers, T.; Smets, J.; Zeegers-Huyskens, Th.; Maes, G. *J. Mol. Struct.* **1991**, *243*, 37.
- (35) Maes, G. In *Intermolecular Forces. An Introduction to Modern Methods and Results*; Huyskens, P., Luck, W. A. P., Zeegers-Huyskens Th., Eds.; Springer Verlag: New York, 1991; pp 195-216.
- (36) Vranken, H. M.Sc. Thesis, University of Leuven, 1992.
- (37) Hallam, H. E.; Scrimshaw, G. F. In *Vibrational Spectroscopy of Trapped Species*; Hallam, H. E., Ed.; Wiley: London, 1973; pp 11-66.
- (38) Maes, G.; Zeegers-Huyskens, Th. *J. Mol. Struct.* **1983**, *100*, 305.